JGR Atmospheres

RESEARCH ARTICLE
10.1029/2023JD039675

Impacts of Atlantic and Pacific Multidecadal Variability on South American Precipitation and Temperature in the CESM Simulations and Observations

Zhaoxiangrui He[1], Aiguo Dai[1], and Mathias Vuille[1]

[1]Department of Atmospheric and Environmental Sciences, University at Albany, State University of New York, Albany, NY, USA

Key Points:

- The Community Earth System Model version 2 improves monsoon rainfall response to Pacific and Atlantic variability compared to version 1
- Precipitation anomaly patterns over South America are related to anomalous subtropical moisture flux and equatorial vertical motion
- Over water-limited regions, anomalies in temperature and precipitation are anti-correlated, possibly due to surface evaporative cooling

Correspondence to:
Z. He,
hzxrkb@gmail.com

Citation:
He, Z., Dai, A., & Vuille, M. (2024). Impacts of Atlantic and Pacific multidecadal variability on South American precipitation and temperature in the CESM simulations and observations. *Journal of Geophysical Research: Atmospheres*, *129*, e2023JD039675. https://doi.org/10.1029/2023JD039675

Received 19 JULY 2023
Accepted 6 JUN 2024

Abstract The Community Earth System Model version 1 (CESM1) and version 2 (CESM2)'s abilities to simulate the impacts of Atlantic multidecadal variability (AMV) and Pacific multidecadal variability (PMV) on South American precipitation and temperature have not been assessed, and how the AMV and PMV modulate each other's influences on South American climate is not well understood. Here we use observations, reanalyses, and CESM1 and CESM2 simulations from 1920 to 2015 to study those problems. The models can reproduce the observed precipitation and temperature responses to AMV well, but can only roughly reproduce such responses to PMV. The precipitation response over the South Atlantic convergence zone (SACZ) is better simulated by CESM2 compared to CESM1, which is associated with an improved horizontal moisture flux over this region. However, the models cannot accurately simulate the observed differences between the influences of Pacific interannual and multidecadal variability on South American precipitation and temperature. The impacts of AMV and PMV on South American precipitation are modulated by the other mode via changes in horizontal moisture flux over the SACZ and River Plate basin in summer, as well as changes in vertical motion over the equatorial regions in winter. Similarly, the impacts of AMV and PMV on South American temperature are also modulated by the other mode. Over water-limited regions, such as northeastern Brazil and southern Argentina, the precipitation and temperature responses are anti-correlated, possibly via surface evaporation.

Plain Language Summary How the Community Earth System Model version 1 and version 2 simulate the influences of Atlantic and Pacific multidecadal sea surface temperature variations on South American climate has not previously been examined, and how the Atlantic and Pacific multidecadal variability (AMV and PMV) modulates the effects from the other basin on South American precipitation and temperature is unclear. In this study, we analyze historical observations and model simulations during 1920–2015 to investigate those problems. The general patterns of the precipitation and temperature responses to AMV are well simulated by both versions of the model, but the patterns of the responses to PMV are only roughly reproduced by the models. The precipitation response over the South American monsoon region is better represented in the model's version 2 than in version 1. The Atlantic and Pacific variability modulates each other's impacts on South American precipitation and temperature. The variations in the patterns of precipitation response are related to changes in horizontal moisture transport over subtropical regions in summer and vertical motion over equatorial regions in winter. The precipitation and temperature responses are anti-correlated over relatively dry regions, such as northeastern Brazil and southern Argentina, possibly through surface evaporation.

1. Introduction

Sea surface temperatures (SST) in the Atlantic and Pacific Oceans vary on interannual to multidecadal time scales, with the El Niño-Southern Oscillation (ENSO)-related interannual variations being dominant in the Pacific (Zhang et al., 1997) and the Atlantic multidecadal variability (AMV) being most pronounced in North Atlantic SSTs (Zhang et al., 2019). In addition to ENSO, Pacific multidecadal variability (PMV) is also evident in Pacific SSTs. The PMV is a decadal-to-multidecadal quasi-oscillation with SST anomaly patterns similar to ENSO, but with comparatively stronger (weaker) SST anomalies (SSTA) in the extratropical (tropical) Pacific (Dong et al., 2018; Liu, 2012; Zhang et al., 1997). The temporal variations of PMV are usually described by the Interdecadal Pacific Oscillation (IPO) index (Dong et al., 2018; Power et al., 1999), or the Pacific Decadal Oscillation (PDO) index for its North Pacific component (Zhang et al., 1997). The IPO and PDO will both be referred to as the PMV, and the IPO index will be used as the PMV index hereafter. The AMV is a multidecadal

quasi-oscillation in North Atlantic SST whose spatial pattern is characterized by horseshoe-like warming (for its warm phase) or cooling (for its cold phase) in the North Atlantic and weaker SSTA of the opposite sign in the South Atlantic (Liu, 2012; Sutton et al., 2018; Zhang et al., 2019). It is also known as the Atlantic Multidecadal Oscillation (AMO; Folland et al., 1984; Schlesinger & Ramankutty, 1994), although AMO may refer to the internally generated component of the AMV in some studies, while the AMV includes both the internally generated and externally-forced multidecadal variations in North Atlantic SSTs (He et al., 2023; Qin et al., 2020). Hereafter, we will refer to the North Atlantic total multidecadal variability as AMV.

The ENSO, PMV, and AMV significantly influence South American climate. El Niño events tend to decrease precipitation over northern and northeastern South America and increase precipitation over southeastern South America, western Ecuador, and central Chile; La Niña events have the opposite influences on South American rainfall (e.g., Cai et al., 2020; Dai & Wigley, 2000; Grimm, 2003, 2011; Zhou & Lau, 2001). The warm-phase PMV, which is associated with a warmer eastern tropical Pacific and a cooler central North Pacific, reduces (increases) annual precipitation over northern South America (southeastern South America and northern Argentina) (Barreiro et al., 2014; Dai, 2013; Dong & Dai, 2015; Flantua et al., 2016; Garreaud et al., 2009; Grimm & Saboia, 2015; Grimm et al., 2016). The PMV-associated precipitation anomalies from December to May over the northern half of South America in Coupled Model Intercomparison Project Phase 5 (CMIP5) model simulations are consistent with the observed patterns (Villamayor et al., 2018). He et al. (2021) showed a similar PMV-related pattern for December–January–February (DJF) precipitation, but it is different for June–July–August (JJA) precipitation. Over extratropical South America, the PMV-related precipitation anomalies result from the Pacific-South American pattern (Karoly, 1989; Mo & Paegle, 2001), which represents atmospheric stationary Rossby wave trains that propagate from the South Pacific Ocean toward eastern South America. The ENSO index is positively correlated with annual surface air temperature (SAT) over most of tropical and subtropical South America (Flantua et al., 2016; Garreaud et al., 2009), while the PMV index is negatively correlated with annual, DJF, and JJA SAT over the central Amazon basin and northeastern South America and positively correlated with SAT over western South America, including the central and northern Andes (Dong & Dai, 2015; He et al., 2021), consistent with the influence of PDO on Andean temperature (Vuille et al., 2015).

The warm-phase AMV is associated with negative anomalies in annual and seasonal precipitation over northeastern South America and Brazil between 10°S and 0°, and positive precipitation response over the northern Amazon basin (Flantua et al., 2016; Knight et al., 2006). Villamayor et al. (2018) showed similar rainfall anomalies associated with the AMV over the northern half of South America but for the wet season in CMIP5 models. He et al. (2021) documented similar anomaly patterns for both DJF and JJA precipitation. The precipitation anomalies over tropical South America result from anomalous atmospheric circulation associated with AMV-related SST anomalies in the tropical North Atlantic. During the AMV warm phase, the warmer tropical North Atlantic displaces the Atlantic Intertropical Convergence Zone (ITCZ) northward and weakens the South American summer monsoon (Knight et al., 2006; Zhou & Lau, 2001), which reduces precipitation over the southeastern Amazon basin and Northeast Brazil, but enhances rainfall over the northeastern Amazon during March–April–May (Flantua et al., 2016; Grimm & Saboia, 2015; Grimm et al., 2016; Hastenrath & Heller, 1977; Hua et al., 2019; Maksic et al., 2022; Nobre & Shukla, 1996). Furthermore, Flantua et al. (2016) and He et al. (2021) showed that SAT over most of tropical South America tends to be warmer than normal during the AMV warm phase.

He et al. (2021) used observations and reanalyses to study the joint impacts of AMV and PMV on South American precipitation and temperature, that is, how the impacts of AMV and PMV on South American precipitation and temperature change with the phase of the other mode. In this study, we further investigate the physical processes that underpin the joint impacts of AMV and PMV on South American precipitation and temperature. We also evaluate Community Earth System Model version 1 (CESM1) and version 2 (CESM2)'s abilities to simulate the influences of AMV and PMV on South American precipitation and temperature and improvements in model performance from CESM1 to CESM2, which has not been done before. Section 2 introduces the data and methods used in this study. Section 3 describes the results. A summary and the main conclusions are presented in Section 4.

2. Data and Methods

2.1. Datasets of Observations, Reanalyses, and Model Simulations

To study the CESM1 and CESM2's abilities to simulate the individual and joint impacts of AMV and PMV on South American climate and investigate the associated processes, we analyzed monthly data of SST,

Table 1
Monthly Datasets Used in This Study

Name and description	Source (reference)	Period	Spatial resolution
20CRv3 Atmospheric reanalysis	https://psl.noaa.gov/data/gridded/data.20thC_ReanV3.html (Slivinski et al., 2019)	1920–2015	1° × 1°
CAM5 Atmospheric simulations (10 runs)	https://www.cesm.ucar.edu/working-groups/climate/simulations/cam5-prescribed-sst (CVCWG, 2020a)	1920–2015	0.9° × 1.25°
CAM6 Atmospheric simulations (10 runs)	https://www.cesm.ucar.edu/working-groups/climate/simulations/cam6-prescribed-sst (CVCWG, 2020b)	1920–2015	0.9° × 1.25°
CRU TS *P* & SAT observations	https://crudata.uea.ac.uk/cru/data/hrg/cru_ts_4.07/ (Harris et al., 2020)	1920–2015	0.5° × 0.5°
ERA5 Atmospheric reanalysis	https://doi.org/10.24381/cds.6860a573 https://doi.org/10.24381/cds.f17050d7 (Hersbach et al., 2023a, 2023b)	1940–2019	0.25° × 0.25°
ERSSTv4 SST observations	https://doi.org/10.7289/V5KD1VVF (Huang et al., 2015)	1920–2019	2° × 2°
ERSSTv5 SST observations	https://doi.org/10.7289/V5T72FNM (Huang et al., 2017)	1920–2019	2° × 2°
GISTEMP SAT observations	https://data.giss.nasa.gov/gistemp/ (GISTEMP Team, 2024; Lenssen et al., 2019)	1920–2015	2° × 2°
GPCC *P* observations	https://doi.org/10.5676/DWD_GPCC/FD_M_V2022_050 (Schneider et al., 2022)	1920–2015	0.5° × 0.5°
GPCP *P* observations	https://doi.org/10.7289/V56971M6 (Adler et al., 2016)	1998–2015	2.5° × 2.5°
TRMM *P* observations	https://doi.org/10.5067/TRMM/TMPA/MONTH/7 (TRMM, 2011)	1998–2015	0.25° × 0.25°

Note. *P* is the abbreviation for precipitation.

precipitation, SAT, and atmospheric fields from model simulations, observations, and atmospheric reanalyses. Table 1 summarizes the datasets used in this study.

Two ensembles of experiments using prescribed SST and ice forcing in CESM1 and CESM2, respectively, were analyzed. First, we used the Community Atmosphere Model version 5.2 (CAM5; Neale et al., 2012) global prescribed SST Atmospheric Model Intercomparison Project (AMIP) ensemble provided by the National Center for Atmospheric Research (NCAR) (CVCWG, 2020a), which contains 10 ensemble runs forced with time-varying observed SST and sea ice over the global oceans from 1920 to 2015. The simulations were conducted using CESM1.1 with CAM5 as its atmospheric component. The AMIP simulations were constrained by historical SST and sea ice, thus excluding ocean-atmosphere-ice feedbacks in the climate system but leaving the atmosphere and land coupled. The atmospheric radiative forcing is based on historical forcing over 1920–2005 and representative concentration pathway 8.5 (RCP8.5; Moss et al., 2010) over 2006–2015. The Extended Reconstructed Sea Surface Temperature version 4 (ERSSTv4; Huang et al., 2015) and Hadley Centre Sea Ice and Sea Surface Temperature version 1 (HadISST1; Rayner et al., 2003) were used, respectively, to specify global SST and sea-ice concentration from 1920 to 2015 in the CAM5 runs.

Second, the 10-member Community Atmosphere Model version 6 (CAM6; Danabasoglu et al., 2020) global prescribed SST AMIP ensemble conducted by NCAR (CVCWG, 2020b) was also used. The simulations were run based on CESM2.1.2, whose atmospheric component is CAM6. The historical forcing was applied to the model from 1920 to 2014; the shared socio-economic pathway 3–7.0 (SSP3; O'Neill et al., 2014, 2017) was used to drive the model over 2015–2021. SST and sea ice in the model were set to the time-varying global SST from the Extended Reconstructed Sea Surface Temperature version 5 (ERSSTv5; Huang et al., 2017) and sea-ice concentration from the HadISST1. Please note that the CAM6 AMIP ensemble's historical forcing ends in 2014 while the CAM5 AMIP ensemble's historical forcing ends in 2006.

Observations of precipitation and temperature as well as atmospheric reanalyses were used to evaluate the models' abilities. We used observed monthly precipitation from the Global Precipitation Climatology Centre (GPCC) version 2022 (Schneider et al., 2022) and the Climatic Research Unit (CRU) Time Series (TS) version 4.07 (Harris et al., 2020), as well as monthly SAT from the CRU TS and the Goddard Institute for Space Studies (GISS) Surface Temperature Analysis (GISTEMP) version 4 (Lenssen et al., 2019; GISTEMP Team, 2024). Atmospheric fields from two reanalyses, the Twentieth Century Reanalysis version 3 (20CRv3; Slivinski et al., 2019) and the European Centre for Medium-Range Weather Forecasts (ECMWF) Reanalysis version 5 (ERA5; Hersbach et al., 2023a, 2023b), were also used. We also used monthly precipitation from the Global Precipitation Climatology Project (GPCP) version 2.3 (Adler et al., 2016) and the Tropical Rainfall Measuring Mission (TRMM) version 7 (TRMM, 2011), which are merged satellite-gauge products, to compare them with modeled precipitation over both continents and oceans.

2.2. Indices of Atlantic and Pacific SST Variability

The Atlantic and Pacific SST indices are similar to those used in He et al. (2021). We used the tripole index (TPI; Henley et al., 2015) as the Pacific SST index:

$$\mathrm{TPI} = \mathrm{SSTA}_2 - \frac{\mathrm{SSTA}_1 + \mathrm{SSTA}_3}{2}, \tag{1}$$

where the SSTA_i ($i = 1, 2, 3$) refers to the linearly detrended (annual or seasonal) SST anomalies (relative to the 1920–2015 mean) from the ERSSTv4 or ERSSTv5 averaged over each of the three TPI regions: $i = 1$ for the western-central North Pacific (25°N–45°N, 140°E−145°W), $i = 2$ for the central-eastern equatorial Pacific (10°S–10°N, 170°E−90°W), and $i = 3$ for the western-central South Pacific (50°S–15°S, 150°E−160°W).

We defined the Atlantic SST index as the linearly detrended (annual or seasonal) SST anomalies (relative to the 1920–2015 mean) from the ERSSTv4 or ERSSTv5 averaged over the North Atlantic (0–60°N, 0–80°W) following Enfield et al. (2001) and Trenberth and Shea (2006). This Atlantic SST index includes all nonlinear variations, including both internally generated variations and externally-forced changes (He et al., 2023; Qin et al., 2020). The SST data from the ERSSTv4 and ERSSTv5 were used to compute the Pacific and Atlantic SST indices over the period 1920–2019, since they were used to force the CAM5 and CAM6 prescribed SST AMIP ensembles, respectively. We also used the Atlantic North–South SST gradient (ANSG) to measure the meridional SST gradient over the tropical Atlantic, according to Hua et al. (2019). The ANSG was defined as the 11-year moving average of the linearly detrended (annual or seasonal) SSTA difference between the tropical North (15°–75°W, 5°–25°N) and South (40°W–20°E, 5°S–25°S) Atlantic. While linearly detrending the data at each grid point can eliminate most of the forced signal driven by external forcing, this method cannot remove decadal variations in external forcing, such as aerosol forcing.

The time series of the Atlantic or Pacific SST index includes interannual variations that are relatively weak in the North Atlantic but dominant in the Pacific. We applied the 11-year moving average to the time series of the Atlantic or Pacific SST index to obtain the time series that represents the multidecadal variability in the North Atlantic (i.e., AMV) or Pacific (i.e., PMV). The Atlantic and Pacific SST indices (which are unsmoothed) as well as the AMV and PMV indices (which are smoothed) from 1920 to 2019 are displayed in Figure 1. The Atlantic SST index's amplitude is close to the AMV index's, but the Pacific SST index's amplitude is much larger than the PMV index's (Figure 1). This suggests that the Atlantic SST variations are dominated by AMV while the Pacific SST variations are dominated by ENSO. The Atlantic and Pacific SST indices include variability across all timescales, while the AMV and PMV indices include mostly the decadal-multidecadal variability.

2.3. Composite Analysis

We used composite analysis to reveal the temperature, precipitation, and atmospheric circulation anomalies associated with different phase combinations of the unsmoothed or smoothed Atlantic and Pacific SST indices. The SST indices based on ERSSTv4 (ERSSTv5) were used to calculate the composites of CAM5 AMIP (CAM6 AMIP, observations, and reanalysis) data. He et al. (2021) described the method in detail, so it is only briefly summarized here. He et al. (2021) used this method to study the joint impacts of AMV and PMV on South American precipitation and temperature in observations and the related anomalous atmospheric circulation in

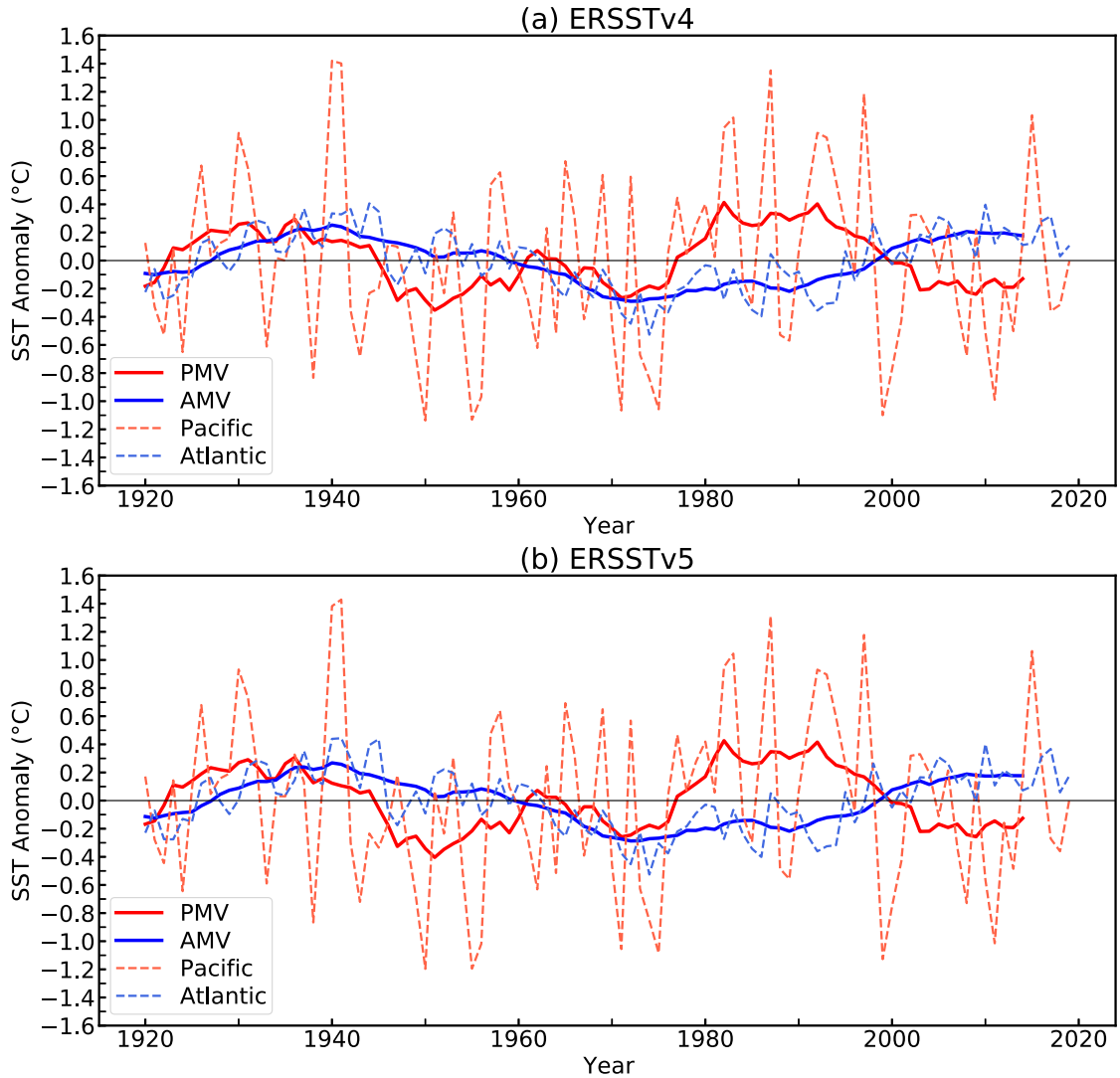

Figure 1. The time series of the annual Atlantic multidecadal variability and Pacific multidecadal variability indices during 1920–2014, as well as the annual Atlantic and Pacific sea surface temperatures indices during 1920–2019 based on the (a) ERSSTv4 and (b) ERSSTv5.

reanalysis data. Here we used this method to assess the CESM1 and CESM2's abilities to simulate the impacts of AMV and PMV on South American climate and to evaluate CESM2's performance compared to observations and CESM1.

First, we converted all the time series of (annual or seasonal) data into anomalies relative to the mean of the analysis period, which is from 1920 to 2015, except for ERA5 which has a different time period (i.e., 1940–2019; Table 1). The anomalies were linearly detrended in order to focus on the nonlinear variations. Then, the data used to construct the composites associated with multidecadal variability were smoothed using an 11-year moving average. For SST, precipitation, and temperature observations, as well as CAM5 and CAM6 AMIP simulations, the data over the period 1915–1919 (2011–2015) were used to calculate the 11-year moving averaged data over the period 1920–1925 (2005–2010). Second, we constructed the composites of the variables using the unsmoothed or smoothed Pacific and Atlantic SST indices. We used "P" and "A" to represent the Pacific and Atlantic, and "w", "n", and "c" as subscripts to represent the warm, neutral, and cold phases of the Pacific and Atlantic SST variability, respectively. For example, Pw represents the warm phase of the Pacific SST variability, and Ac represents the cold phase of the Atlantic SST variability. We grouped the years into the warm case when the respective index is $>0.5\sigma$ (σ is the standard deviation of the time series of the index) and the cold case when the

Table 2
The Years and Means of AMV and PMV Indices for the Smoothed Cases During 1920–2010 Based on ERSSTv5

Case name	Years (number of years)	Mean of PMV index	Mean of AMV index
Pw	1923, 1925–1940, 1979–1998 (37)	0.242	−0.030
Pc	1920, 1921, 1946–1960, 1966, 1969–1976, 2003–2010 (34)	−0.217	−0.007
Aw	1930–1949, 1956, 2001–2010 (31)	−0.010	0.164
Ac	1920–1925, 1965–1996 (38)	0.093	−0.177
PwAw	1930–1940 (11)	0.209	0.183
PwAc	1923, 1925, 1979–1996 (20)	0.275	−0.154
PcAw	1946–1949, 1956, 2003–2010 (13)	−0.215	0.141
PcAc	1920, 1921, 1966, 1969–1976 (11)	−0.182	−0.229

Note. The standard deviations of the AMV and PMV indices are 0.159°C and 0.215°C, respectively.

index is $<-0.5\sigma$, and all other years fall into the neutral case. The use of 0.5σ allows reasonable sampling of the different cases examined here. We then obtained the composites for the cases Pw, Pn, Pc, Aw, An, and Ac for each variable. These composites were obtained based on the SST index in the Pacific or Atlantic only, regardless of the phase of the SST variability in the other basin. Typically, the Pacific (Atlantic) SST index has a small mean value (i.e., nearly neutral) when averaged across all years within the case Aw or Ac (Pw or Pc) (He et al., 2021; Tables 2 and 3). Third, considering the Pacific and Atlantic SST indices together, we grouped the years into the nine possible phase combinations of Atlantic and Pacific SST variability: PnAn, PwAn, PcAn, PnAw, PnAc, PwAw, PcAw, PwAc, and PcAc. For example, PwAn represents years when a warm-phase Pacific mode coincided with a neutral-phase Atlantic mode. Tables 2 and 3 list the years included in the various composite cases for the smoothed data and unsmoothed data, respectively. Fourth, we calculated the difference of the means of composites to obtain the response of a variable to the Pacific or Atlantic SST anomalies during the neutral, warm, and cold phases of the other mode. The composite differences Pw − Pc and Aw − Ac are similar to the composite differences PwAn − PcAn and PnAw − PnAc, respectively, except that the latter cases include fewer years. In other words, the average phase of the Atlantic (Pacific) mode in the case Pw or Pc (Aw or Ac) is nearly neutral, making it possible to use the composite difference Pw − Pc (Aw − Ac) to represent the impacts of Pacific (Atlantic) SST variability under the neutral conditions in the Atlantic (Pacific). We use the composite differences

Table 3
The Years and Means of Atlantic and Pacific SST Indices for the Unsmoothed Cases During 1920–2019 Based on ERSSTv5

Case name	Years (number of years)	Mean of Pacific SST index	Mean of Atlantic SST index
Pw	1926, 1930, 1931, 1936, 1940, 1941, 1953, 1957, 1958, 1965, 1966, 1969, 1972, 1977, 1980, 1982, 1983, 1986, 1987, 1991–1994, 1997, 2002, 2003, 2015 (27)	0.726	−0.041
Pc	1922, 1924, 1933, 1938, 1942, 1943, 1945, 1949, 1950, 1954–1956, 1962, 1964, 1967, 1970, 1971, 1973–1975, 1988, 1989, 1999–2001, 2007, 2008, 2010, 2011, 2013, 2018 (31)	−0.676	−0.005
Aw	1926, 1927, 1931–1933, 1936–1942, 1944, 1945, 1951–1953, 1955, 1958, 1960, 1998, 2003–2008, 2010, 2012, 2013, 2016, 2017, 2019 (33)	0.025	0.241
Ac	1920, 1922–1925, 1947, 1964, 1965, 1967, 1968, 1970–1978, 1982, 1984–1986, 1991–1994, 1996 (28)	0.006	−0.272
PwAw	1926, 1931, 1936, 1940, 1941, 1953, 1958, 2003 (8)	0.728	0.239
PwAc	1965, 1972, 1977, 1982, 1986, 1991–1994 (9)	0.676	−0.317
PcAw	1933, 1938, 1942, 1945, 1955, 2007, 2008, 2010, 2013 (9)	−0.600	0.239
PcAc	1922, 1924, 1964, 1967, 1970, 1971, 1973–1975 (9)	−0.675	−0.266

Note. The standard deviations of the Atlantic and Pacific SST indices are 0.218°C and 0.592°C, respectively.

Pw − Pc and Aw − Ac to represent, respectively, the impacts of Pacific and Atlantic SST variations during the neutral phase of the other mode; we use the composite differences PwAw − PcAw and PwAw − PwAc to represent, respectively, the Pacific and Atlantic impacts during the warm phase of the other mode; and we use the composite differences PwAc − PcAc and PcAw − PcAc to represent, respectively, the Pacific and Atlantic impacts during the cold phase of the other mode. This method is similar to the approach of Enfield et al. (2001), who compared the correlations between ENSO and the rainfall over the continental United States during the warm and cold periods of the AMV. The composites could also be used to study the combined effects of AMV and PMV on South American climate. For example, the composite PcAw represents the combined impacts of cold-phase PMV and warm-phase AMV. Such analyses have been conducted in prior studies by Grimm et al. (2016) and Kayano et al. (2022), and we revisit this issue later in the next section (Figure 5). Please note that for the cases of unsmoothed data, the Pacific influence is dominated by ENSO-related interannual variations, while the Atlantic influence originates mainly from the AMV, as the interannual variability of the average of North Atlantic SSTA is relatively small. Tables 2 and 3 show that the magnitude of the (unsmoothed) Pacific SST index is two to three times larger than the magnitude of the (unsmoothed) Atlantic SST index during their warm or cold phases, but the magnitudes of the PMV and AMV indices are comparable. These magnitudes of SST variations are relevant for the precipitation and temperature anomalies over South America discussed below.

2.4. Significance Tests

The statistical significance of the difference between the means of composites was assessed using a bootstrap method (Efron, 1979; Zwiers, 1990) which estimates the distribution of the difference through random resampling 10,000 times. Specifically, suppose from a time series X we create two sub-samples X_A (e.g., for AMV warm phase) with n_A data points and X_B (e.g., for AMV cold phase) with n_B data points, whose sample means are μ_A and μ_B. We randomly resample X (with replacement, i.e., one individual can be sampled more than once) to obtain two bootstrap samples X_A^1 with n_A data points and X_B^1 with n_B data points and calculate their means as μ_A^1 and μ_B^1. We repeat this process 10,000 times and obtain the bootstrap samples $X_A^1, X_A^2, \ldots, X_A^{10000}, X_B^1, X_B^2, \ldots, X_B^{10000}$, and their means $\mu_A^1, \mu_A^2, \ldots, \mu_A^{10000}, \mu_B^1, \mu_B^2, \ldots, \mu_B^{10000}$. The differences between the means of bootstrap samples $\mu_A^1 - \mu_B^1$, $\mu_A^2 - \mu_B^2, \ldots, \mu_A^{10000} - \mu_B^{10000}$ represent an empirical bootstrap distribution of the difference between sample means. We determine whether the difference $\mu_A - \mu_B$ is statistically significant (i.e., not by chance) by comparing it with the 2.5th or 97.5th percentile of the empirical bootstrap distribution. That is, if $\mu_A - \mu_B$ is above the 97.5th percentile or below the 2.5th percentile of the distribution, which has a mean of almost zero, then the difference $\mu_A - \mu_B$ is statistically significant, that is, the μ_A and μ_B are significantly different at the 5% significance level (or 95% confidence level).

2.5. Moisture Flux Convergence

To investigate the contribution of variations in atmospheric circulation to precipitation variations, we analyzed the vertically integrated horizontal moisture flux and its convergence. The horizontal moisture flux integrated between 1,000 and 200 hPa is

$$F = \frac{1}{g}\int_{200\ \mathrm{hPa}}^{1000\ \mathrm{hPa}} \mathbf{v}q\, dp \tag{2}$$

and the horizontal moisture flux convergence integrated between 1,000 and 200 hPa is:

$$\mathrm{Conv} = -\frac{1}{g}\int_{200\ \mathrm{hPa}}^{1000\ \mathrm{hPa}} \nabla(\mathbf{v}q)\, dp. \tag{3}$$

In the equations, the fields $\mathbf{v}$ (=u, v), q, and p are horizontal winds, specific humidity, and pressure, respectively. The standard constant g is the gravitational acceleration at the surface of the Earth.

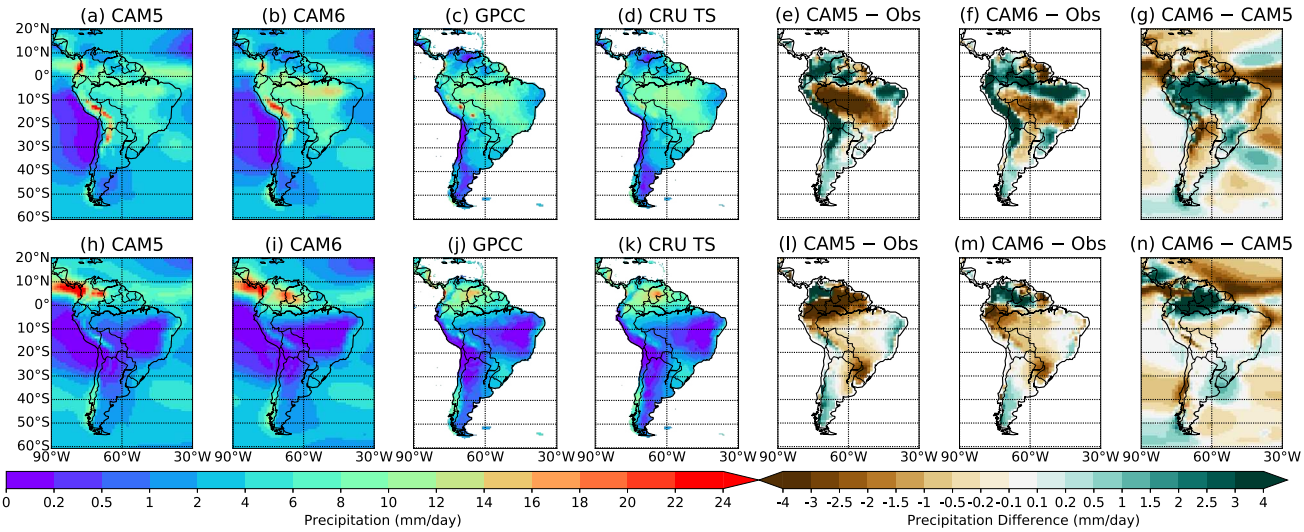

Figure 2. The DJF precipitation climatology over 1920–2015 from the (a) CAM5 and (b) CAM6 AMIP simulations, (c) GPCC, and (d) CRU TS. The difference in DJF precipitation climatology over 1920–2015 between (e) CAM5 AMIP ensemble and the observations (i.e., the average of precipitation climatologies in GPCC and CRU TS), (f) CAM6 AMIP ensemble and the observations, and (g) CAM6 and CAM5 AMIP ensembles. Panels (h–n) same as panels (a–g) but for JJA.

3. Results

3.1. The Impacts of Pacific SST Variability on South American Precipitation

In this section, we compare the impacts of Pacific SST variability on South American precipitation during the warm, neutral, and cold phases of North Atlantic SST variability from the CAM5 and CAM6 AMIP simulations with those from the observations, and investigate the associated processes through an analysis of atmospheric circulation anomalies. We also compare the results derived from the smoothed data associated with decadal variations with those obtained from the unsmoothed data which reflect primarily the influence of ENSO. Please note that the CAM5 and CAM6 AMIP simulations were run using CESM1 and CESM2 respectively, therefore we use the phrases CAM5 and CESM1 as well as CAM6 and CESM2 interchangeably.

The CESM1 and CESM2's performance on simulating the South American monsoon has been examined by Meehl et al. (2020). They showed that the December–January–February–March precipitation in CESM2 is stronger over 0°–10°S Brazil compared to CESM1. The accompanied 850-hPa winds recurve to the southeast more (i.e., the low-level easterlies are weaker) over 0°–10°S in South America in CESM2 than in CESM1. As a result, the simulated precipitation over the western and southern Amazon basin, Bolivian Andes, and South Atlantic Convergence Zone (SACZ) agrees with observations better in CESM 2 than in CESM1, while the opposite is true for the modeled precipitation over northeastern and southeastern South America, and the Peruvian Andes. To help better understand the models' ability of simulating South American precipitation responses to AMV and PMV, we plot the DJF and JJA South American precipitation climatology from the CAM5 and CAM6 AMIP simulations (Figures 2a, 2b, 2h, and 2i) and observations (GPCC and CRU TS; Figures 2c, 2d, 2j, and 2k); we also show the two models' deficiencies (Figures 2e, 2f, 2l, and 2m) and the difference between the CAM6 and CAM5 (Figures 2g and 2n).

Figures 3a–3l show the impacts of PMV on South American DJF precipitation during different AMV phases from the CAM5 and CAM6 AMIP simulations, GPCC, and CRU TS. During the neutral AMV phase, the warm-phase PMV decreases DJF precipitation over most of northern South America, but increases it over eastern Brazil and northern Argentina in both models and observations, although the CAM5 does not show a precipitation increase over southeastern Brazil and the CAM6 shows weak responses over eastern Brazil and northern Argentina (Figures 3a–3d). The observed patterns are noisier than those in He et al. (2021), because the latter uses precipitation values averaged across three observational datasets. Figures 3e–3h (Figures 3i–3l) represent the impacts from the PMV modulated by the AMV warm (cold) phase plus the influences from the concurring Atlantic SSTA. The effect from Atlantic SSTA would be canceled out to a large extent in the composite difference PwAw –

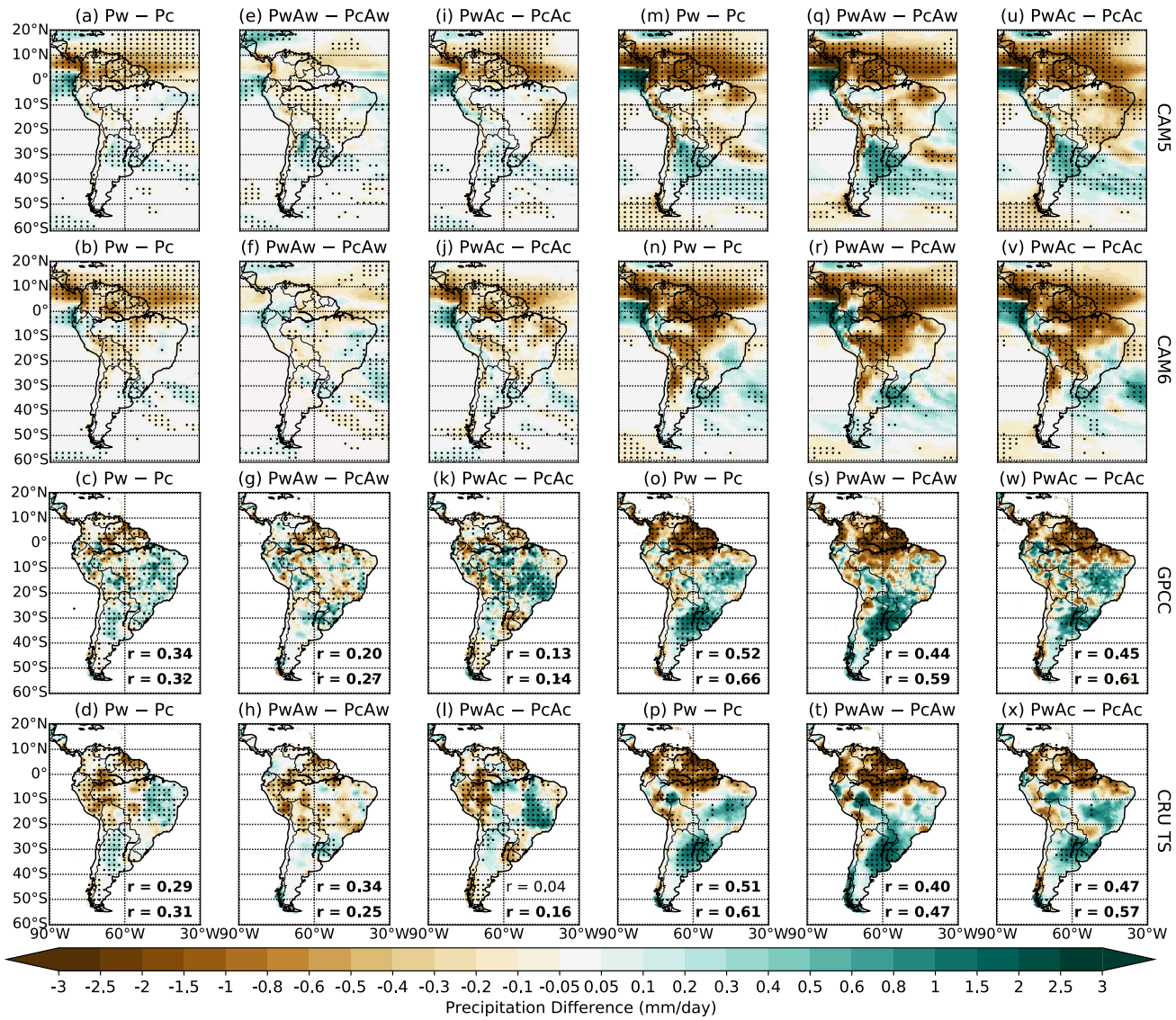

Figure 3. Left three columns (a–l): The impacts of Pacific multidecadal variability on South American DJF precipitation during the (a–d) neutral, (e–h) warm, and (i–l) cold Atlantic multidecadal variability phases based on smoothed and linearly detrended data during 1920–2010 from the (first row) CAM5 AMIP simulations, (second row) CAM6 AMIP simulations, (third row) GPCC, and (fourth row) CRU TS. Right three columns (m–x): Same as the left three columns but based on unsmoothed and linearly detrended data during 1920–2015, which reflect mainly the influence of ENSO. Stippling indicates regions where the precipitation difference is above the 95% confidence level. The third and fourth rows include the spatial pattern correlation coefficients between the panel and the (upper) first-row panel and (lower) second-row panel in the same column. The spatial pattern correlations that are above the 95% confidence level are indicated by bold text. The observational data were remapped to the models' grids before calculating the spatial correlations.

PcAw or PwAc − PcAc if the influence of PMV on Atlantic SST is small. However, this is not the case, the AMV index is larger in the composites PwAw and PwAc than in the composites PcAw and PcAc respectively (Table 2), which may be because the warm-phase PMV could warm tropical Atlantic and hence increase the AMV index (Meehl et al., 2021). During the warm (cold) AMV phase, the PMV-related DJF precipitation anomalies from the central Amazon basin to central-eastern Brazil are more negative (positive) than they are during the neutral AMV phase, while they are more positive (negative) over southern Brazil and Uruguay, implying a weakening (strengthening) of the SACZ (Figures 3g, 3h, 3k, and 3l). The increase (reduction) in PMV-related precipitation difference over the SACZ (southeastern South America) under a cold-phase AMV background (Figures 3k and 3l) may be related to the low-level anomalous cyclonic circulation over southeastern Brazil (not shown), because such anomalous circulation is associated with the strengthened moisture flux from the Amazon basin toward the

SACZ and the weakened moisture flux from the Amazon basin to the River Plate basin (Tedeschi et al., 2015). The model results generally agree with the observations for the impacts of PMV during the AMV neutral and warm phase (Pw − Pc and PwAw − PcAw), but fail to reproduce the observed wetting from the central Amazon basin to southeastern Brazil when the AMV is in its cold phase (PwAc − PcAc) (Figures 3a, 3b, 3e, 3f, 3i, and 3j). Overall, CAM6 performs slightly better than CAM5 when reproducing these cases.

The unsmoothed data, which reflect primarily the influence of ENSO (Figure 1), show similar but stronger anomaly patterns compared to the smoothed data (i.e., decadal variations) (Figure 3). The models and observations show more pronounced and widespread dry anomalies over northern South America and wet anomalies over southeastern South America for the unsmoothed anomalies compared to the smoothed anomalies (Figure 3). These anomalies are due to the eastward shift of the descending branch of the Walker circulation toward eastern equatorial South America and the western equatorial Atlantic (Espinoza et al., 2016; Grimm, 2003; Sasaki et al., 2015; Zhou & Lau, 2001), as well as high-pressure anomalies over eastern subtropical South America related to the PSA pattern (Karoly, 1989; Mo & Paegle, 2001). The results from the models are broadly consistent with those from the observations, except for the lack of enhanced rainfall over central-eastern Brazil seen in observations (CAM6 reproduces the correct sign of the rainfall response). CAM6 reproduces the weak positive difference over southeastern Brazil but fails to simulate the positive values over northeastern Argentina. The observations show that during the warm (cold) phase of Atlantic SST variability, the Pacific SST variability-related precipitation differences are more negative (positive) over the SACZ, and more (less) positive over southeastern South America than during the neutral phase of Atlantic SST variability (Figures 3o, 3p, 3s, 3t, 3w, and 3x), which resembles the impacts of eastern (central) Pacific El Niño events on South American DJF precipitation (Cai et al., 2020; Tedeschi et al., 2015). The modulation effects of Atlantic SST variability on precipitation over the SACZ and southeastern South America are likely through changing moisture flux convergence over these regions. Specifically, compared to the neutral phase of Atlantic SST variability (Figures 4a–4d), the Pacific SST variability-related horizontal moisture flux convergence differences are more negative (positive) over the SACZ during the warm (cold) phase of Atlantic SST variability, while the opposite is true for the moisture flux convergence differences over the River Plate basin (Figures 4e–4h and 4i–4l). This implies reduced (increased) moisture convergence over the SACZ and enhanced (weakened) moisture convergence over the subtropical plains during the warm (cold) phase of Atlantic SST variability. The moisture convergence over the SACZ is associated with low-level winds and horizontal moisture flux from the Amazon basin, while the moisture convergence over the River Plate basin is related to moisture transport from central South America (Figure 4). The models can simulate the general patterns of low-level winds and moisture flux changes, and CAM6 simulates such changes over the SACZ much better than CAM5 (Figures 4a, 4b, 4e, 4f, 4i, and 4j; Figure 14 of Meehl et al., 2020), which explains why the precipitation response over the SACZ in CAM6 is improved in comparison to CAM5. This improvement might be related to an increase in the sensitivity of deep convection to lower tropospheric moisture, an increase in the magnitude of 850-hPa winds from the equatorial Andes and Amazon basin toward the southeastern part of the continent (Meehl et al., 2020), and a better representation of the South Pacific Convergence Zone (SPCZ) in CESM2 compared to CESM1. The SPCZ is a band of low-level convergence, cloudiness and precipitation extending from the Western Pacific Warm Pool at the maritime continent southeastward to 30°S, 120°W (Brown et al., 2020), and closely connected with SACZ activity via Rossby-wave propagation from the South Pacific toward South America, thereby influencing the position and intensity of the upper-level trough that maintains the SACZ (Grimm & Silva Dias, 1995). Indeed, the long-term means of annual SST (Figure 8 of Meehl et al., 2020) and DJF precipitation (not shown) over the SPCZ are higher in CESM2 than in CESM1, with the former being in better agreement with the observations.

Both the PMV and AMV were in their warm phases from the late 1920s to the middle 1940s, and they were both in their cold phases from the middle 1960s to the middle 1970s (Figure 1), which corresponds to the first mode of South American summer precipitation in Grimm and Saboia (2015) and Grimm et al. (2016). The observations show that the combined effects of the warm-phase PMV and AMV (i.e., the composite difference between the combinations of warm-phase PMV with warm-phase AMV and cold-phase PMV with cold-phase AMV) would enhance precipitation over western Colombia and Ecuador, southern Chile, the central-southern Amazon basin, and the SACZ, and reduce precipitation over the rest of South America (Figures 5c and 5d). The CAM6 simulations reproduce the precipitation responses over the SACZ and northeastern Brazil, while both CAM5 and CAM6 fail to simulate the precipitation response over Argentina (Figures 5a and 5b). Moreover, a combination of warm-phase PMV and cold-phase AMV occurred from the late 1970s to the late 1990s, and a combination of

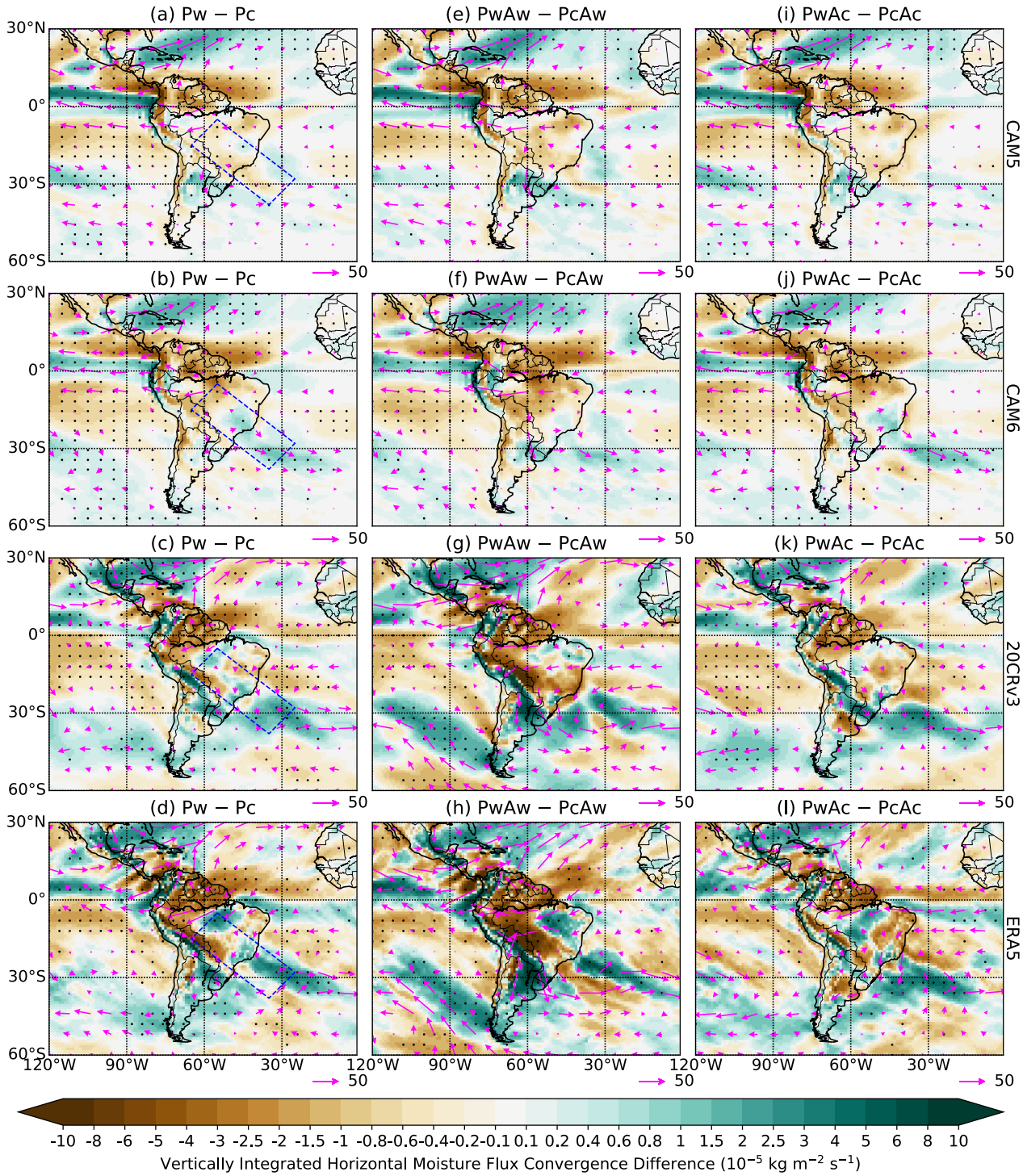

Figure 4. The impacts of Pacific sea surface temperatures (SST) variability on South American DJF horizontal moisture flux convergence integrated between 1,000 and 200 hPa ($-\frac{1}{g}\int_{200\ \mathrm{hPa}}^{1000\ \mathrm{hPa}} \nabla(\mathbf{vq})\,\mathrm{dp}$) during the (a–d) neutral, (e–h) warm, and (i–l) cold phases of the Atlantic SST variability based on unsmoothed and linearly detrended data from the (first row) CAM5 AMIP simulations, (second row) CAM6 AMIP simulations, and (third row) 20CRv3 during 1920–2015, and from the (fourth row) ERA5 during 1940–2019. Positive (negative) values indicate convergence (divergence) of moisture flux associated with horizontal winds. Stippling indicates regions where the vertically integrated horizontal moisture flux convergence difference is above the 95% confidence level. The pink vectors show the horizontal moisture flux integrated between 1,000 and 200 hPa ($\frac{1}{g}\int_{200\ \mathrm{hPa}}^{1000\ \mathrm{hPa}} \mathbf{vq}\,\mathrm{dp}$) in the unit of kg m^{-1} s^{-1} for each case. The dashed blue box in (a–d) indicates the climatological position of the SACZ.

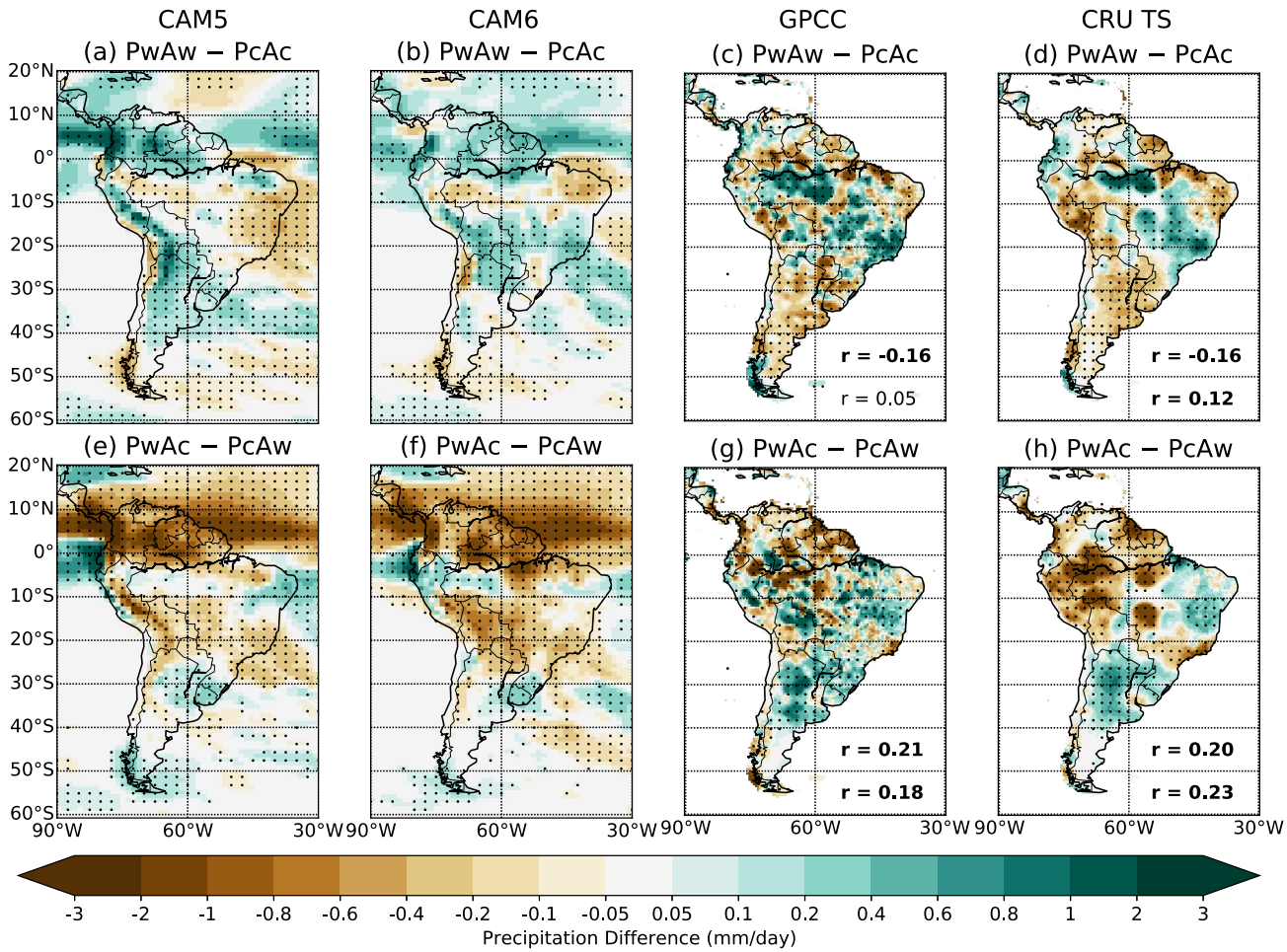

Figure 5. The South American DJF precipitation responses to the combined effects of (a–d) the same phases of the Pacific multidecadal variability (PMV) and Atlantic multidecadal variability (AMV) and (e–h) the opposite phases of the PMV and AMV based on smoothed and linearly detrended data during 1920–2010 from the (a, e) CAM5 AMIP simulations, (b, f) CAM6 AMIP simulations, (c, g) GPCC, and (d, h) CRU TS. Stippling indicates regions where the precipitation difference is above the 95% confidence level. The spatial pattern correlation coefficients between the observations and the (upper) CAM5 simulations and (lower) CAM6 simulations are displayed in c-d and g-h. The spatial pattern correlations that are above the 95% confidence level are indicated by bold text.

cold-phase PMV and warm-phase AMV occurred from the early 2000s to the middle 2010s (Figure 1), which corresponds to the second mode of summer precipitation over South America in Grimm and Saboia (2015) and Grimm et al. (2016). The combined effects of the warm-phase (cold-phase) PMV and cold-phase (warm-phase) AMV over the period 1976–2015 would decrease (increase) northern South American summer precipitation, and increase (reduce) precipitation over eastern and southeastern South America (Figures 5g and 5h). The models can reproduce the precipitation response over northern and southeastern South America, but struggle to simulate the precipitation response over the rest of South America (Figures 5e and 5f). Our results based on observations are consistent with the results of Grimm and Saboia (2015), Grimm et al. (2016), and Kayano et al. (2022).

Next, we analyze how the AMV modulates the influence of PMV on South American precipitation during JJA, which represents the wet season in South America north of the equator and southernmost South America, but is the dry season with little precipitation over tropical and subtropical South America south of the equator. Overall, CAM6 improves the representation of the JJA precipitation climatology when compared to CAM5 (Figure 2).

The effects of PMV on South American JJA precipitation (Figures 6a–6l) are weaker than those on DJF precipitation (Figures 3a–3l). The observed PMV-related JJA precipitation anomalies are generally weak and poorly simulated by the models (Figures 6a–6l). When the AMV is in its neutral phase, the warm-phase PMV reduces JJA precipitation over equatorial South America, and increases precipitation slightly over parts of northern South

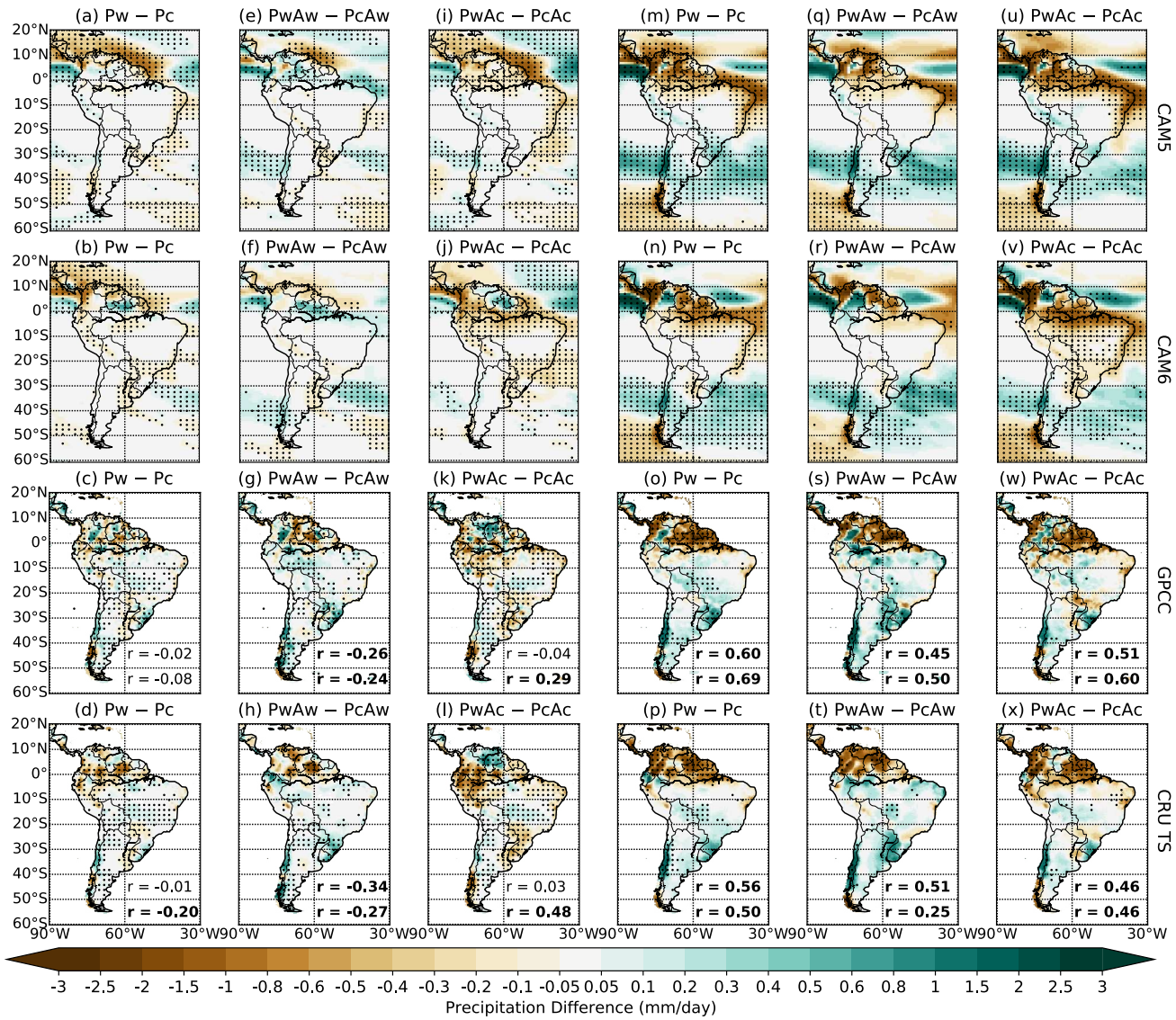

Figure 6. Same as Figure 3 but for JJA precipitation.

America, southern Brazil, and central Chile (Figures 6a–6d). When the AMV is in its cold phase, the precipitation differences become more negative over equatorial South America, southern Brazil, and southern-central Chile, and more positive over Venezuela compared to the neutral and warm AMV phases (Figures 6a–6d, 6e–6h, and 6i–6l). The variations in equatorial South American precipitation response might correspond to changes in the ANSG, since a positive (negative) ANSG anomaly tends to displace the Atlantic ITCZ northward (southward) and induce anomalous subsidence (convection) over equatorial South America. We found that the values of ANSG for the cases Pw − Pc, PwAw − PcAw, and PwAc − PcAc are −0.079°C, −0.083°C, and 0.138°C, respectively. In the CAM5 simulations, the weakened (enhanced) PMV-induced drying effect over equatorial South America during the warm (cold) AMV phase is located farther north relative to the observations, while CAM6 correctly reproduces this effect (Figures 6e–6h and 6i–6l).

The large-scale changes seen in the observed unsmoothed JJA precipitation response to Pacific SST anomalies during the different phases of Atlantic SST variability are stronger than the smoothed case, and they are correctly simulated by the models (Figures 6m–6x). The Pacific SST variability-related precipitation differences over northern South America (around the equator in the models, and over 0°–10°N in the observations) are consistent with the vertical velocity differences over this region (Figure 7), which are related to the tropical North Atlantic

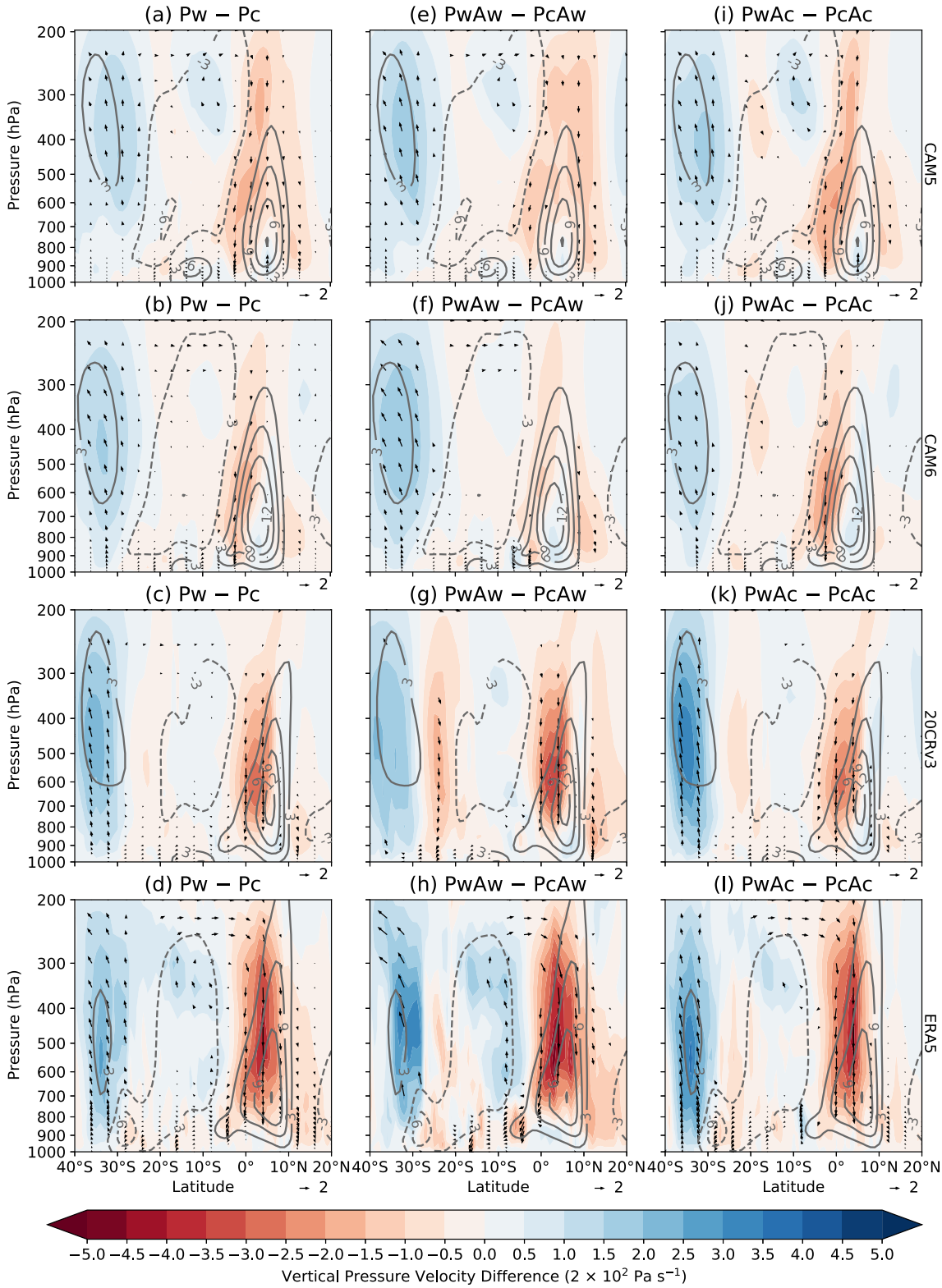

Figure 7.

warming and thus a northward shift of the Atlantic ITCZ caused by the Pacific-North American (PNA) pattern (Horel & Wallace, 1981; Wallace & Gutzler, 1981) through the wind-evaporation-SST feedback (Amaya & Foltz, 2014; Chiang et al., 2002). The anomalous subsidence during the warm phase of Pacific SST variability over northern South America, regardless of the AMV phase, is consistent with earlier studies showing that El Niño contributed to Amazonian droughts in 1983, 1998, and 2010 (Chen et al., 2011; Jiménez-Muñoz et al., 2016; Lewis et al., 2011; Marengo et al., 2011). The anomalous subsidence near the equator is weakened (enhanced) during the warm (cold) AMV phase compared to the neutral AMV phase (Figures 7e–7h and 7i–7l). This indicates weaker (stronger) anomalous descending motion over equatorial South America and hence wetter (drier) conditions over this region when the AMV is in its warm (cold) phase than when the AMV phase is neutral.

3.2. The Impacts of Atlantic SST Variability on South American Precipitation

This section discusses how the impacts of Atlantic SST variability on South American precipitation change with Pacific conditions and examines the corresponding atmospheric circulation anomalies. Moreover, we compare the influences of Atlantic SST variability on South American precipitation during DJF and JJA in the CAM5 and CAM6 AMIP simulations and observations, and compare the results based on smoothed and unsmoothed data.

Figures 8a–8l show the impacts of AMV on South American DJF precipitation during the neutral, warm, and cold PMV phases using the smoothed data. The results from models show wetting over northern South America and east of the central Andes and drying over the southwestern Amazon basin and eastern Brazil during the warm-phase AMV regardless of the PMV phase, which might relate to a northward shift of the Atlantic ITCZ (Figures 8a, 8b, 8e, 8f, 8i, and 8j). The observations show more spatial variations with increased precipitation over the western-central Amazon basin, western Colombia, and Guyana, and drying over northeastern Brazil during the neutral phase of PMV (Figures 8c and 8d). The observations also show drying over northern Argentina during the AMV warm phase (Figures 8c and 8d), which is not simulated by the models. The CAM5 is unable to adequately reproduce much of the impacts of AMV on South American DJF precipitation, which are quite noisy, as highlighted by the very low spatial correlations between the model and observations, regardless of the phase of PMV. The precipitation response over the SACZ is better simulated by CAM6 than by CAM5. The model deficiency of precipitation over northeastern Brazil might be related to the model deficiency of the Atlantic ITCZ (not shown) and SST (Figure 8 of Meehl et al., 2020). In the observations, the effects of AMV (Figures 8c and 8d) are roughly the opposite of the impacts of PMV (Figures 3c and 3d), which might be due to the warm-phase AMV-induced La Niña-like SSTA in the Pacific (Cai et al., 2019; Meehl et al., 2021). Figures 8e–8h (Figures 8i–8l) represent the impacts from AMV modulated by the PMV warm (cold) phase and the impacts from the concurring Pacific SSTA. The effect from the concurring Pacific SSTA would be mostly eliminated when the two composites (i.e., PwAw and PwAc or PcAw and PcAc) are subtracted if the AMV has little effect on Pacific SST. However, the PMV index for PwAw (PcAw) is smaller than that for PwAc (PcAc; Table 2). Such differences are consistent with the influences of AMV on the Pacific SST (with Aw leading to Pc) through inter-basin teleconnections (Cai et al., 2019; Johnson et al., 2020; Meehl et al., 2021; Ruprich-Robert et al., 2017, 2021; Zhang & Delworth, 2007). In the observations, during the warm (cold) PMV phase, the DJF precipitation differences from the central Amazon basin to southeastern Brazil (i.e., SACZ) are more negative (positive), and the precipitation differences over southeastern South America and southern Chile are more positive (negative) than during the neutral PMV phase (Figures 8g, 8h, 8k, and 8l). The more positive (negative) AMV-related precipitation response over the SACZ (southeastern South America) during the cold-phase PMV (Figures 8k and 8l) might be related to the low-level anomalous cyclonic circulation over southeastern Brazil (not shown), because such anomalous circulation could enhance ascending motion over the SACZ, and cause anomalous moisture transport convergence (divergence) over the SACZ (River Plate basin) (Tedeschi et al., 2015). Neither CAM5 nor CAM6 correctly reproduces the variations in precipitation response to the warm-phase AMV during different phases of the PMV over the SACZ and southeastern South America (Figures 8e, 8f, 8i, and 8j).

Figure 7. The impact of Pacific sea surface temperatures (SST) variability on JJA vertical velocity averaged over the 75°–35°W sector (color shading, positive values indicate upward motion) and JJA local Hadley circulation averaged over the 75°–35°W sector (vectors, shown where either meridional or vertical wind difference is above the 95% confidence level) during the (a–d) neutral, (e–h) warm, and (i–l) cold phases of the Atlantic SST variability based on unsmoothed and linearly detrended data from the (first row) CAM5 AMIP simulations, (second row) CAM6 AMIP simulations, and (third row) 20CRv3 during 1920–2015, and from the (fourth row) ERA5 during 1940–2019. A scaling factor of −200 was applied to the vertical pressure velocity (Pa/s) for visualization. The contours show the climatologies of vertical velocity with an interval of −600 Pa/s. Solid contours indicate positive values, dashed contours indicate negative values, and the zero-contour line is omitted.

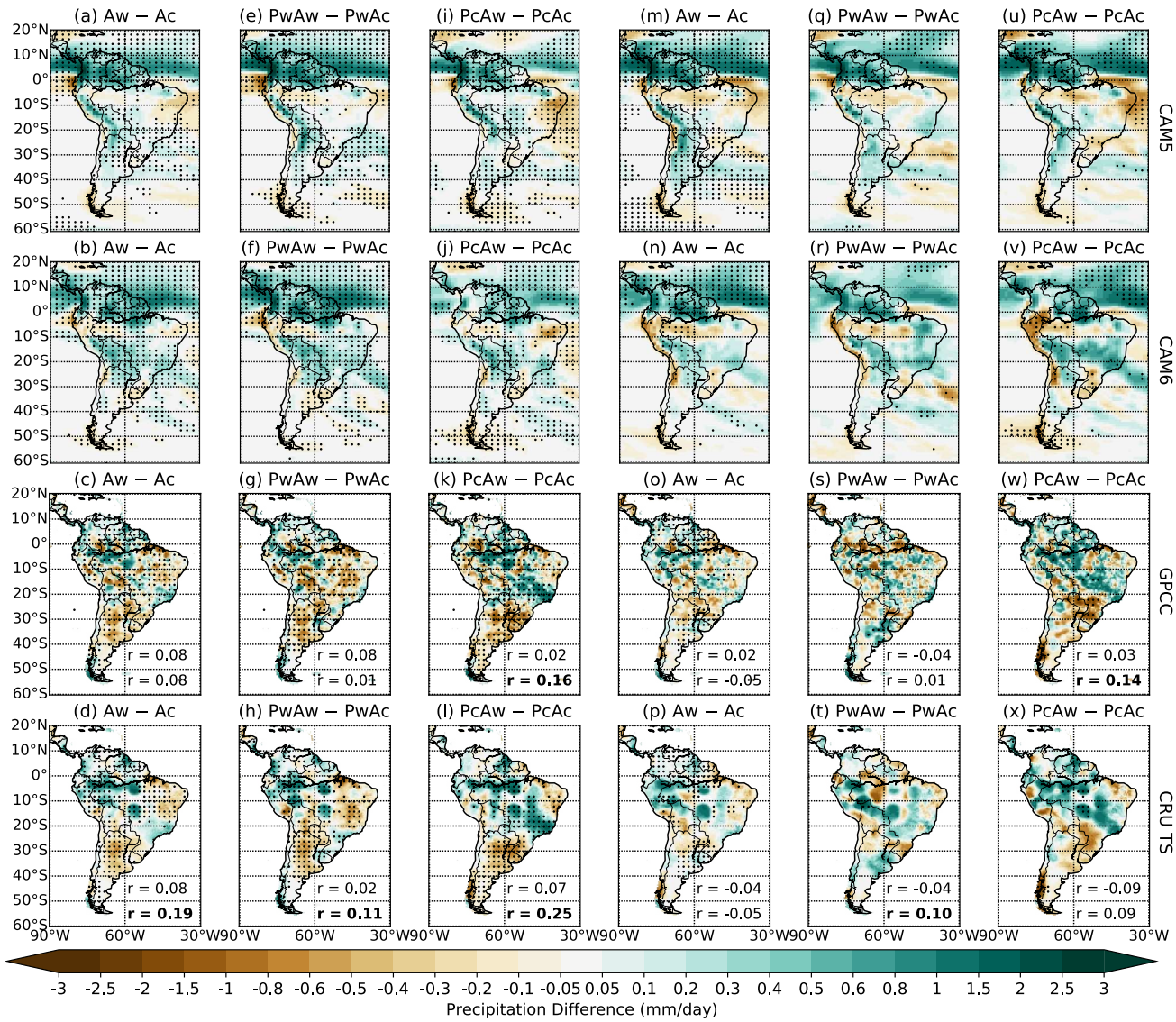

Figure 8. Left three columns (a–l): The impacts of Atlantic multidecadal variability on South American DJF precipitation during the (a–d) neutral, (e–h) warm, and (i–l) cold Pacific multidecadal variability phases based on smoothed and linearly detrended data during 1920–2010 from the (first row) CAM5 AMIP simulations, (second row) CAM6 AMIP simulations, (third row) GPCC, and (fourth row) CRU TS. Right three columns (m–x): Same as the left three columns but based on unsmoothed and linearly detrended data during 1920–2015. Stippling indicates regions where the precipitation difference is above the 95% confidence level. The third and fourth rows include the spatial pattern correlation coefficients between the panel and the (upper) first-row panel and (lower) second-row panel in the same column. The spatial pattern correlations that are above the 95% confidence level are indicated by bold text. The observational data were remapped to the models' grids before calculating the spatial correlations.

For the unsmoothed data, the impacts of Atlantic SST variability on South American DJF precipitation during warm and cold phases of the Pacific SST variability are similar to the results for the smoothed data from both the models and observations (Figure 8). This is expected as the time series of North Atlantic SSTA is dominated by decadal-multidecadal variations, rather than interannual variations, unlike the Pacific SSTs (Figure 1). The models simulate the effect of Atlantic SST variability on precipitation over most of South America poorly, as in the smoothed case. The models produce a response to the Atlantic SST variability that is zonally oriented between 10°S and 10°N, with increased precipitation north of the Amazon River and a decrease to the south (Figures 8m, 8n, 8q, 8r, 8u, and 8v). The phase of the Pacific SST variability does not significantly affect the precipitation response to the Atlantic SSTA in the CAM5 simulations (Figures 8m, 8q and 8u). In the CAM6 simulations and observations, the Atlantic SST variability-induced horizontal moisture flux convergence anomalies are more

positive over the SACZ during the cold phase of Pacific SST variability than during the neutral or warm phase of Pacific SST variability (Figures 9b–9d, 9f–9h, and 9j–9l) which might lead to wetting over the SACZ (Figures 8n–8p, 8r–8t, and 8v–8x). The moisture flux convergence differences over the River Plate basin are more positive (negative) when the Pacific SST variability is in its warm (cold) phase compared to its neutral phase (Figures 9b–9d, 9f–9h, and 9j–9l), which is consistent with the precipitation response over this region (Figures 8n–8p, 8r–8t, and 8v–8x). However, the anomalous moisture flux convergence over the SACZ in the CAM6 simulations (Figures 9b, 9f, and 9j) is much weaker than in the reanalysis data (Figures 9c, 9d, 9g, 9h, 9k, and 9l). This result suggests that CAM6 improves the precipitation response to Atlantic SST variability over the SACZ and southeastern South America compared to CAM5, although the magnitude of the response is still underestimated relative to the observations. This improvement might be related to a better representation of deep convection, tropical South American low-level winds, and the SPCZ in CAM6 compared to CAM5, as discussed in Section 3.1.

Next, we discuss the impacts of AMV on South American JJA precipitation during different PMV phases (Figures 10a–10l). Again, the JJA precipitation responses are relatively weak but more spatially coherent compared with DJF precipitation, and the model results show weak responses over most of South America south of the equator. The models correctly simulate the influence of AMV over northern South America and southern Brazil, but fail to reproduce the drying over other parts of South America. When the PMV is in its neutral phase, the warm-phase AMV decreases JJA precipitation over most of South America in both the models and observations, except over parts of northern and northwestern South America and southern-central Chile, where JJA precipitation increases (Figures 10a–10d). When the PMV is in its warm (cold) phase, the precipitation differences are more positive (negative) compared with the neutral PMV phase over 0°–10°S South America, southeastern South America, and southern-central Chile, and more negative (positive) over Venezuela in observations (Figures 10g, 10h, 10k, and 10l). The models reproduce the variations in precipitation response to AMV over equatorial South America and southern-central Chile under the background of different PMV phases (Figures 10e, 10f, 10i, and 10j). The variations in the influence of AMV on equatorial South American JJA precipitation during the PMV warm (cold) phase might be related to the reduced (enhanced) ANSG, that is, 0.161 (0.382)°C, compared to the ANSG during the PMV neutral phase, that is, 0.257°C. Because the smaller ANSG is conducive to a reduced northward displacement of the Atlantic ITCZ in response to the warm-phase AMV and the opposite is also true, the anomalous descending motion (precipitation) over 0°–10°S South America is weaker (larger) in the case PwAw − PwAc than in the case PcAw − PcAc.

As was the case for DJF precipitation, for the unsmoothed data, the influence of Atlantic SST variability on South American JJA precipitation is similar to the smoothed data, with slightly stronger anomalies (Figures 10m–10x). The agreement between the models and observations is much better than for DJF and for the decadal variations, as indicated by the higher pattern correlations (Figures 10o, 10p, 10s, 10t, 10w, and 10x). The precipitation pattern over equatorial and northern South America is linked to the strength of the regional convection, as shown by the weakened (enhanced) anomalous subsidence over equatorial (in the models) or 0°–10°S (in the reanalyses) South America during the warm (cold) phase of Pacific SST variability compared to its neutral phase (Figure 11). While the strength of this subsidence is affected by the Pacific SST, its origins are associated with the warm phase of Atlantic SST variability. Previous studies have shown that a warmer North Atlantic and a northward displacement of the Atlantic ITCZ would reduce precipitation over the southeastern Amazon basin and Northeast Brazil and enhance rainfall over the northeastern Amazon basin during March–April–May (Hastenrath & Heller, 1977; Hua et al., 2019; Nobre & Shukla, 1996). Some studies (e.g., Malhi et al., 2008; Marengo et al., 2008; Zeng et al., 2008) thus attribute Amazon droughts, such as the one that occurred in 2005, to a warmer tropical North Atlantic.

3.3. The Impacts of Pacific SST Variability on South American Temperature

In this section, we analyze the impacts of Pacific SST variability on South American annual SAT during the neutral, warm, and cold AMV phases in the CAM5 and CAM6 AMIP simulations and observations. We discuss annual SAT rather than seasonal SAT as the patterns of DJF and JJA SAT responses are very similar to each other and to the pattern of annual SAT responses.

For the smoothed data, during the neutral-phase AMV, the warm-phase PMV warms western and eastern South America, and cools middle Brazil from north to south (Figures 12c and 12d). The models fail to simulate the cooling from the northern Amazon basin to southern Brazil (Figures 12a and 12b). The impact of PMV on SAT is

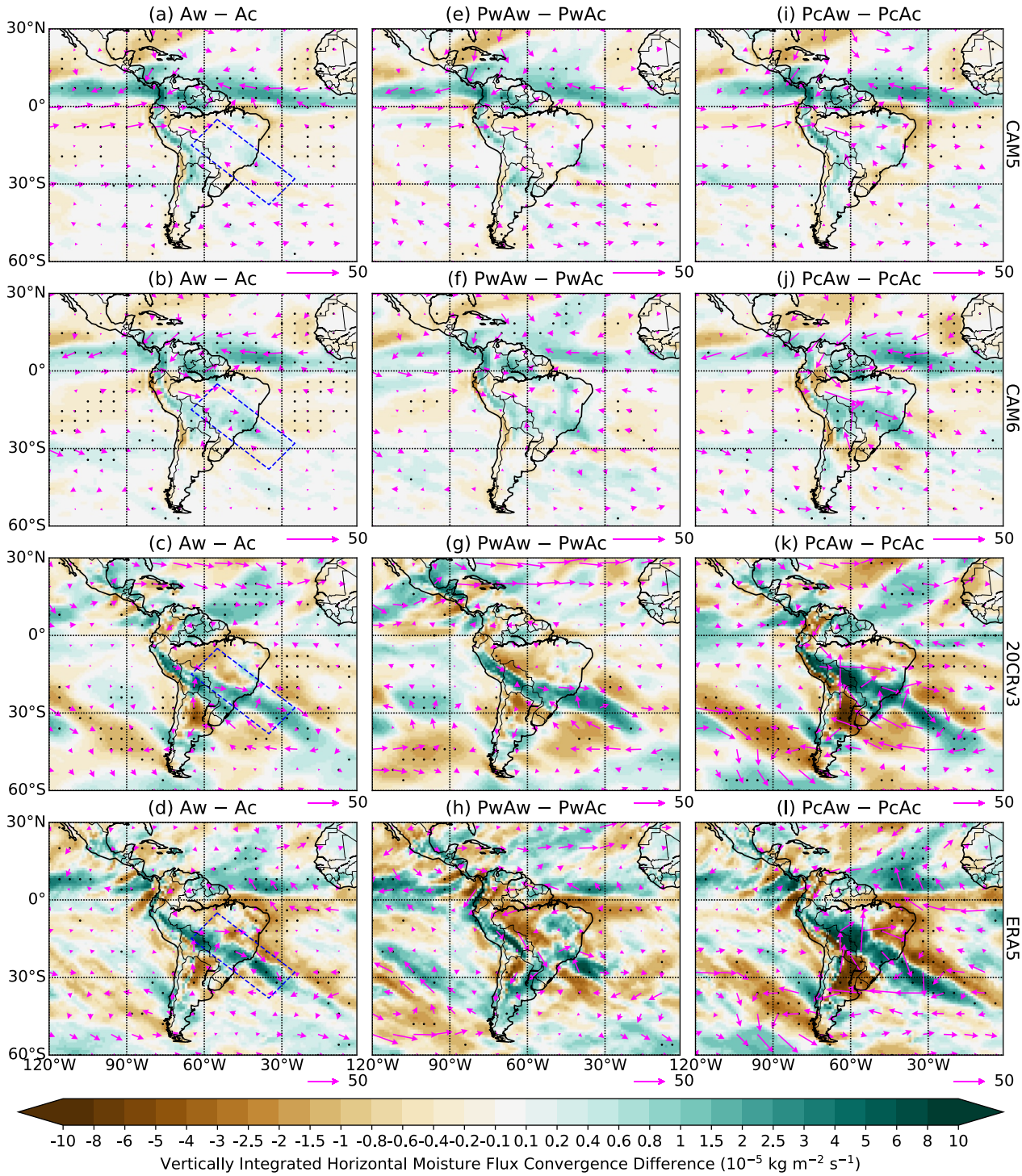

Figure 9. The impacts of Atlantic sea surface temperatures (SST) variability on South American DJF horizontal moisture flux convergence integrated between 1,000 and 200 hPa ($-\frac{1}{g}\int_{200\ \mathrm{hPa}}^{1000\ \mathrm{hPa}} \nabla(\mathbf{v}q)\,dp$) during the (a–d) neutral, (e–h) warm, and (i–l) cold phases of the Pacific SST variability based on unsmoothed and linearly detrended data from the (first row) CAM5 AMIP simulations, (second row) CAM6 AMIP simulations, and (third row) 20CRv3 during 1920–2015, and from the (fourth row) ERA5 during 1940–2019. Stippling indicates regions where the vertically integrated horizontal moisture flux convergence difference is above the 95% confidence level. The pink vectors show the horizontal moisture flux integrated between 1,000 and 200 hPa ($\frac{1}{g}\int_{200\ \mathrm{hPa}}^{1000\ \mathrm{hPa}} \mathbf{v}q\,dp$) in the unit of kg m^{-1} s^{-1} for each case. The dashed blue boxes in (a–d) indicate the climatological position of the SACZ.

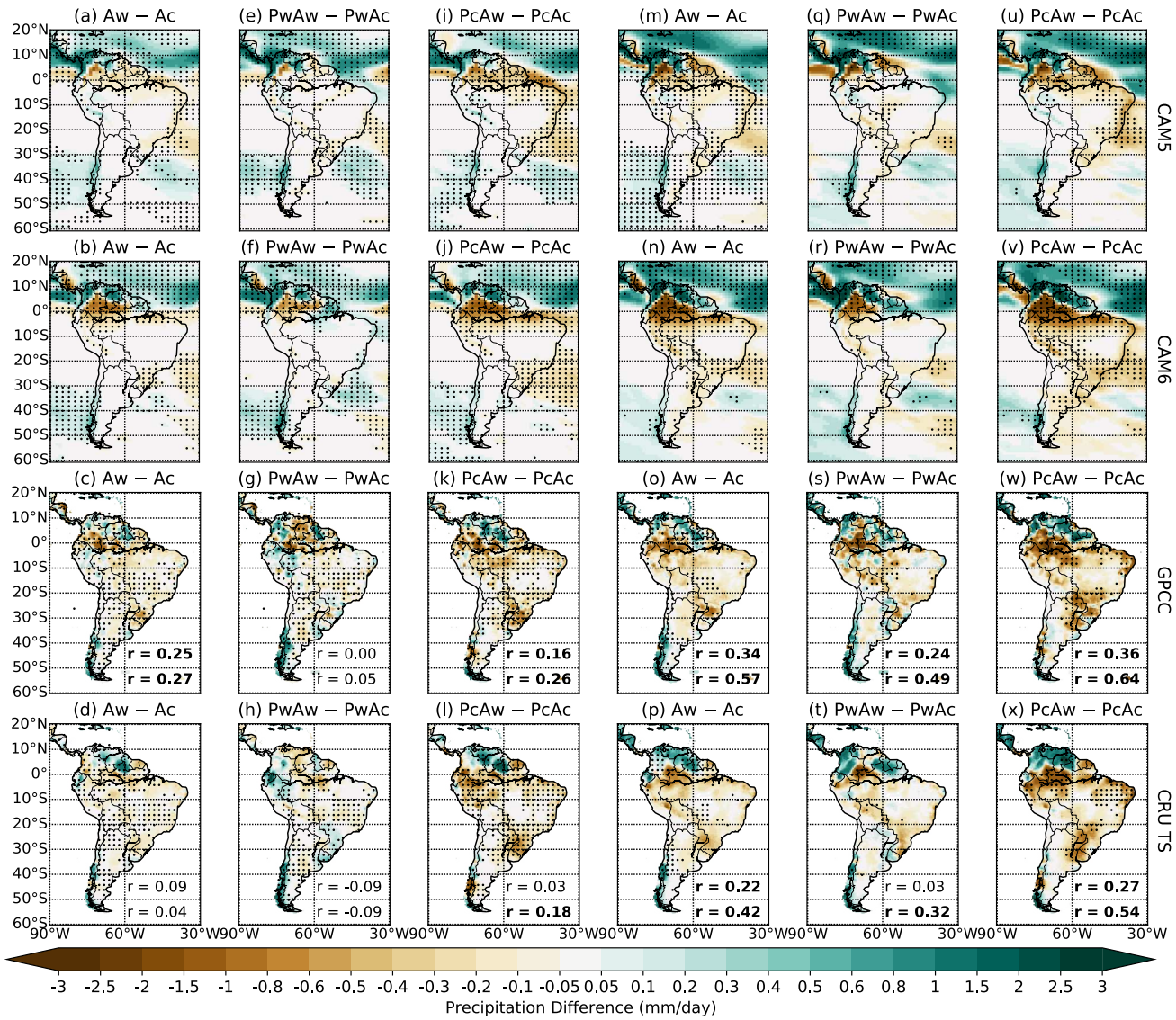

Figure 10. Same as Figure 8 but for JJA precipitation.

more negative (positive) over most of South America during the warm (cold) AMV phase than during the neutral AMV phase (Figures 12e–12h and 12i–12l), which means that the warm anomalies over western and eastern South America get weaker (stronger), while the anomalies over Patagonia get more negative (positive). The models reproduce the variations in SAT anomalies with the PMV phase over western South America, northeast Brazil, and Patagonia. The modulation effect of AMV on the patterns of PMV-induced SAT anomalies over northeastern Brazil and eastern Patagonia appears to be related to the precipitation changes over these regions (e.g., northeastern Brazil in Figures 6e–6h and 6i–6l; eastern Patagonia in Figures 3e–3h and 3i–3l). According to the aridity index (Figure 2 of Zomer et al., 2022), which is defined as the ratio of precipitation to potential evapotranspiration (sometimes the inverse of this ratio is used), northeastern Brazil and Patagonia to the east of the Andes are water-limited regions (i.e., variation of actual evapotranspiration is dominated by precipitation). Precipitation over these regions is substantially less than potential evapotranspiration, therefore it is more likely that a large fraction of precipitation will evaporate rather than infiltrate the soil. As a result, more precipitation in these locations would result in enhanced evaporation and thus lower temperature via evaporative cooling, and the opposite is also true. Previous research has also explored this precipitation-temperature relationship (e.g., Barros et al., 2002; Grimm et al., 2007; Trenberth & Shea, 2005).

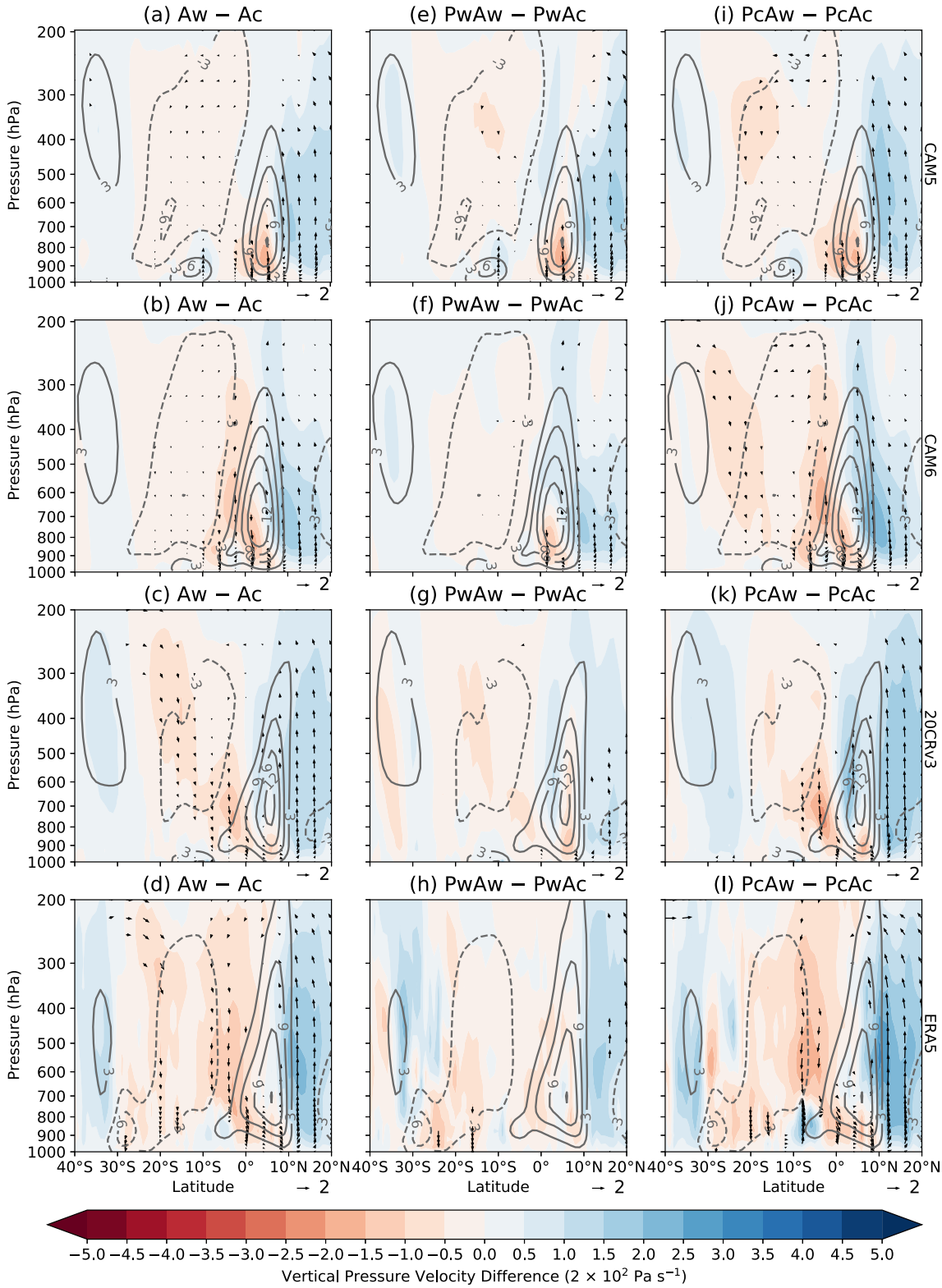

Figure 11.

Unlike for the smoothed cases, the warm-phase Pacific SST variability leads to positive SAT anomalies (by a few tenths of 1°C) over most of South America when considering the unsmoothed cases, except for its southern tip (Figures 12m–12p). When the Atlantic SST variability is in its warm (cold) phase, the warming over the Peruvian Andes and River Plate basin is slightly reduced (enhanced) (Figures 12s, 12t, 12w, and 12x), and the cooling over the southern tip is weaker (stronger) (Figures 12r, 12t, 12v, and 12x). The models overestimate the warming over most of Brazil and the cooling in southernmost South America during the warm phase of Pacific SST variability (Figures 12m, 12n, 12q, 12r, 12u, and 12v).

3.4. The Impacts of Atlantic SST Variability on South American Temperature

This section discusses the impacts of Atlantic SST variability on South American SAT during different phases of Pacific SST variability in the CAM5 and CAM6 AMIP simulations and observations.

Figures 13a–13l show that an AMV warm phase leads to warming (by a few tenths °C) over most of South America during the neutral-phase PMV (Figures 13a–13d), while during the PMV warm (cold) phase these temperature differences are slightly reduced (enhanced) (Figures 13e–13h and 13i–13l). The models simulate the observed broad warming response to the AMV as well as the modulation by the PMV quite well (Figures 13a–13l). Again, there is an apparent anti-correlation between the temperature and precipitation changes over northeastern Brazil and eastern Patagonia (e.g., northeastern Brazil in Figures 10e–10h and 10i–10l; eastern Patagonia in Figures 8g, 8h, 8k, and 8l), where precipitation is more likely to evaporate and cause evaporative cooling given they are highly water-limited regions (Figure 2 of Zomer et al., 2022).

The impacts of Atlantic SST variability on South American annual SAT based on the unsmoothed data are similar to the results of smoothed data (Figures 13m–13x) but with slightly stronger anomalies, which again suggests that the multidecadal variability is dominating the North Atlantic SST variability. The influence of the unsmoothed variations of North Atlantic SST on South American SAT is correctly reproduced by the models.

4. Summary and Discussion

Prior work has documented the impacts of Atlantic and Pacific multidecadal variability on South American climate. However, these studies have not investigated such impacts in CESM. In this study, we performed composite analyses using observations, reanalyses, and CESM1 and CESM2 model simulations from 1920 to 2015 (except for ERA5 which covers 1940–2019), to evaluate the models' ability to reproduce the impacts of AMV and PMV on South American precipitation and temperature, investigate the processes through which the AMV and PMV modulate the influences from the other basin on South American climate, and compare the patterns of South American precipitation or temperature anomalies associated with the smoothed and unsmoothed Pacific and Atlantic SST indices.

In this study we found that during the warm (cold) AMV phase, the PMV's wetting effect in DJF from the central Amazon basin to central-eastern Brazil is suppressed (enhanced), corresponding to suppressed (enhanced) SACZ convective activity, which relates to enhanced (weakened) horizontal moisture flux from tropical South America toward the River Plate basin and reduced (strengthened) moisture flux from Amazonia to central-eastern Brazil. The PMV's drying effect in JJA over equatorial South America is also reduced (enhanced), due to a weaker (stronger) regional subsidence during the warm (cold) AMV phase. The warm (cold) phase of AMV cools (warms) the PMV-related SAT anomalies over most of South America, which is partly related to increased (reduced) precipitation and evapotranspiration over water-limited areas. The modulation of the impacts of AMV on South American precipitation and SAT by the PMV is similar to the modulation effect of AMV on the impacts of PMV. The unsmoothed variations have somewhat different fingerprints but similar modulation effects on precipitation and SAT compared to those in the smoothed variations. These findings extend those of He et al. (2021), showing that variations of the impacts of Pacific or Atlantic SST variability on South American precipitation during different

Figure 11. The impacts of Atlantic sea surface temperatures (SST) variability on JJA vertical velocity averaged over the 75°–35°W sector (color shading, positive values indicate upward motion) and JJA local Hadley circulation averaged over the 75°–35°W sector (vectors, shown where either meridional or vertical wind difference is above the 95% confidence level) during the (a–d) neutral, (e–h) warm, and (i–l) cold phases of the Pacific SST variability based on unsmoothed and linearly detrended data from the (first row) CAM5 AMIP simulations, (second row) CAM6 AMIP simulations, and (third row) 20CRv3 during 1920–2015, and from the (fourth row) ERA5 during 1940–2019. A scaling factor of −200 was applied to the vertical pressure velocity (Pa/s) for visualization. The contours show the climatologies of vertical velocity with an interval of −600 Pa/s. Solid contours indicate positive values, dashed contours indicate negative values, and the zero-contour line is omitted.

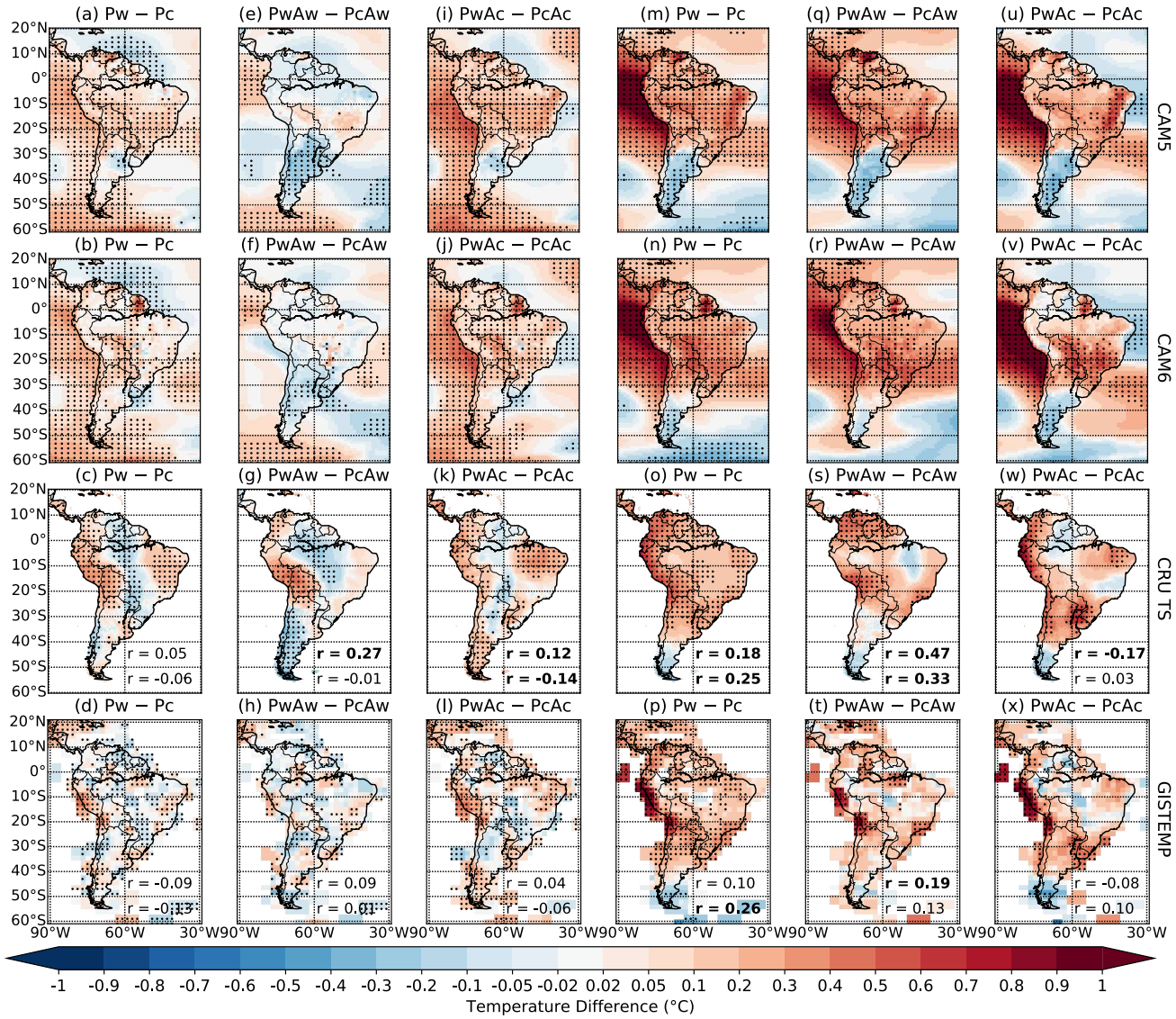

Figure 12. Left three columns (a–l): The impacts of Pacific multidecadal variability on South American annual surface air temperature (SAT) during the (a–d) neutral, (e–h) warm, and (i–l) cold Atlantic multidecadal variability phases based on smoothed and linearly detrended data during 1920–2010 from the (first row) CAM5 AMIP simulations, (second row) CAM6 AMIP simulations, (third row) CRU TS, and (fourth row) GISTEMP. Right three columns (m–x): Same as the left three columns but based on unsmoothed and linearly detrended data during 1920–2015. Stippling indicates regions where the SAT difference is above the 95% confidence level. The third and fourth rows include the spatial pattern correlation coefficients between the panel and the (upper) first-row panel and (lower) second-row panel in the same column. The spatial pattern correlations that are above the 95% confidence level are indicated by bold text. Before computing the spatial correlations between the models and CRU TS (GISTEMP), the data of CRU TS (models) were remapped to the models' grids (GISTEMP's grid).

phases of the other mode are related to changes in moisture flux over subtropical regions and vertical motions over equatorial regions. Our results also suggest the need to apply low-pass filters to extract the correct signals of PMV and consider the responses of South American climate to Atlantic and Pacific SST variations jointly.

We assess, for the first time, CESM1 and CESM2's ability to simulate the responses of South American precipitation and temperature to Atlantic and Pacific SST variability. Observations prior to ∼1960 are sparse in most of South America, which complicates straightforward comparisons between models and observations. The CAM5 and CAM6 model simulations forced with observed SSTs reproduce many of the broad anomaly patterns of South American precipitation and temperature associated with the AMV, although the pattern correlations are not significant in some cases. However, the models can only reproduce a few patterns of the South American precipitation and temperature responses to PMV. The spatial patterns of the Atlantic and Pacific-induced anomalies

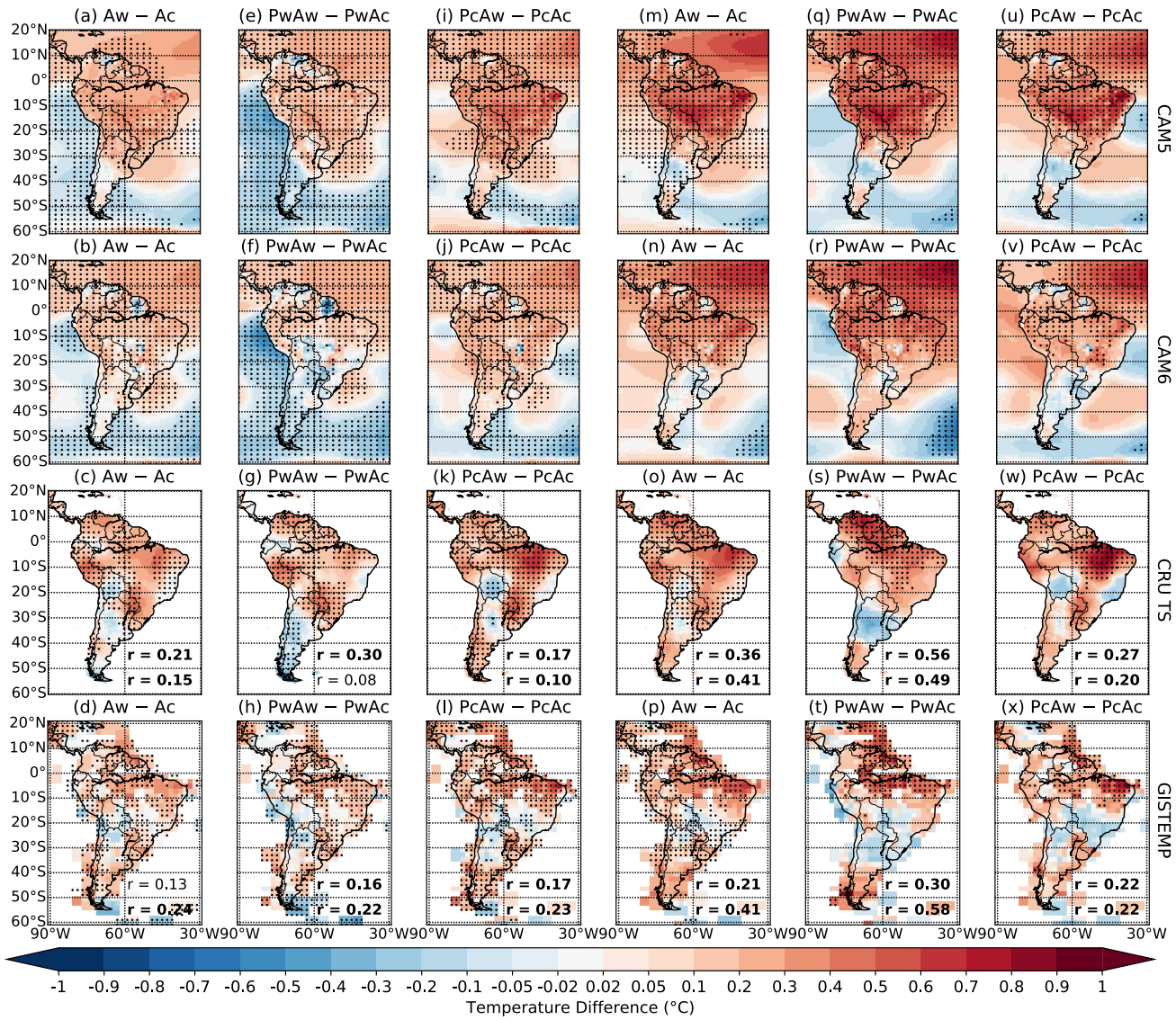

Figure 13. Left three columns (a–l): The impacts of Atlantic multidecadal variability on South American annual surface air temperature (SAT) during the (a–d) neutral, (e–h) warm, and (i–l) cold Pacific multidecadal variability phases based on smoothed and linearly detrended data during 1920–2010 from the (first row) CAM5 AMIP simulations, (second row) CAM6 AMIP simulations, (third row) CRU TS, and (fourth row) GISTEMP. Right three columns (m–x): Same as the left three columns but based on unsmoothed and linearly detrended data during 1920–2015. Stippling indicates regions where the SAT difference is above the 95% confidence level. The third and fourth rows include the spatial pattern correlation coefficients between the panel and the (upper) first-row panel and (lower) second-row panel in the same column. The spatial pattern correlations that are above the 95% confidence level are indicated by bold text. Before computing the spatial correlations between the models and CRU TS (GISTEMP), the data of CRU TS (models) were remapped to the models' grids (GISTEMP's grid).

in South American DJF and JJA precipitation and annual mean temperature during different phases of the variability in the other basin are well captured by CESM1 and CESM2 when using unsmoothed data (except for the Atlantic impacts on DJF precipitation and Pacific impacts on annual temperature). The precipitation responses to Atlantic and Pacific SST variations over the SACZ are improved in CESM2 in comparison to CESM1, which relates to the improvement in simulating deep convection and horizontal moisture flux over the SACZ and convection over the SPCZ. This result indicates that the future projections and paleoclimatic reconstructions for the climate of South American monsoon region based on CESM2 might be improved when compared to CESM1. Unlike the observations, in the CAM5 and CAM6 simulations, the South American precipitation and temperature responses to the Pacific SST variations for the unsmoothed data are similar to those for the smoothed data, but stronger. This suggests that the model cannot differentiate between the impacts of ENSO and PMV on South

American climate. The models also do a better job of simulating the unsmoothed Pacific and Atlantic SST variations' influences on South American precipitation and temperature than the impacts of smoothed Pacific and Atlantic SST variability. This indicates that the models lack some key aspects for correctly simulating atmospheric processes related to decadal-multidecadal variability (especially for the PMV). Future work should further reduce model deficiencies and improve models' representation of South American multidecadal climate variability.

Future work could employ South Pacific atmospheric circulation forcing to explore the relationship between the South Pacific and the variability of the South American monsoon system (Barros & Silvestri, 2002). It would also be of interest to explore the use of the CESM1 Indian Ocean Pacemaker Ensemble to study the influences of the Indian Ocean basin mode, the Indian Ocean dipole, and the subtropical Indian Ocean dipole on South American climate. Finally, the contribution of land use change to South American monsoon variability might be investigated using CESM2 Large Ensemble (Salazar et al., 2015).

Data Availability Statement

All data used in this study are openly available and can be downloaded using the links in Table 1.

Acknowledgments
This study was supported by NSF-PIRE (OISE-1743738) and NSF-P2C2 (EAR-2103041). A. Dai was also supported by NSF Grant AGS-1353740. The authors deeply appreciate CESM Climate Variability & Change Working Group (CVCWG), Copernicus Climate Change Service, CRU, Goddard Earth Sciences Data and Information Services Center, GPCC, National Aeronautics and Space Administration (NASA) GISS, National Oceanic and Atmospheric Administration (NOAA) Climate Program Office, NOAA National Centers for Environmental Information, NOAA Physical Sciences Laboratory, and U.S. Department of Energy Office of Science Biological and Environmental Research for providing the data used in this study. We are also grateful for insightful and constructive comments from two reviewers that helped to significantly improve the quality of this manuscript.

References

Adler, R., Wang, J.-J., Sapiano, M., Huffman, G., Chiu, L., Xie, P.-P., et al. (2016). Global Precipitation Climatology Project (GPCP) Climate Data Record (CDR), version 2.3 (monthly) [Dataset]. *NOAA National Centers for Environmental Information*. https://doi.org/10.7289/V56971M6

Amaya, D. J., & Foltz, G. R. (2014). Impacts of canonical and Modoki El Niño on tropical Atlantic SST. *Journal of Geophysical Research: Oceans*, *119*(2), 777–789. https://doi.org/10.1002/2013JC009476

Barreiro, M., Díaz, N., & Renom, M. (2014). Role of the global oceans and land–atmosphere interaction on summertime interdecadal variability over northern Argentina. *Climate Dynamics*, *42*(7–8), 1733–1753. https://doi.org/10.1007/s00382-014-2088-6

Barros, V. R., Grimm, A. M., & Doyle, M. E. (2002). Relationship between temperature and circulation in southeastern South America and its influence from El Niño and La Niña events. *Journal of the Meteorological Society of Japan*, *80*(1), 21–32. https://doi.org/10.2151/jmsj.80.21

Barros, V. R., & Silvestri, G. E. (2002). The relation between sea surface temperature at the subtropical south-central Pacific and precipitation in southeastern South America. *Journal of Climate*, *15*(3), 251–267. https://doi.org/10.1175/1520-0442(2002)015%3C0251:TRBSST%3E2.0.CO;2

Brown, J. R., Lengaigne, M., Lintner, B. R., Widlansky, M. J., van der Wiel, K., Dutheil, C., et al. (2020). South Pacific Convergence Zone dynamics, variability and impacts in a changing climate. *Nature Reviews Earth & Environment*, *1*(10), 530–543. https://doi.org/10.1038/s43017-020-0078-2

Cai, W., McPhaden, M. J., Grimm, A. M., Rodrigues, R. R., Taschetto, A. S., Garreaud, R. D., et al. (2020). Climate impacts of the El Niño-Southern Oscillation on South America. *Nature Reviews Earth & Environment*, *1*(4), 215–231. https://doi.org/10.1038/s43017-020-0040-3

Cai, W., Wu, L., Lengaigne, M., Li, T., McGregor, S., Kug, J.-S., et al. (2019). Pantropical climate interactions. *Science*, *363*(6430), eaav4236. https://doi.org/10.1126/science.aav4236

Chen, Y., Randerson, J. T., Morton, D. C., Defries, R. S., Collatz, G. J., Kasibhatla, P. S., et al. (2011). Forecasting fire season severity in South America using sea surface temperature anomalies. *Science*, *334*(6057), 787–791. https://doi.org/10.1126/science.1209472

Chiang, J. C. H., Kushnir, Y., & Giannini, A. (2002). Deconstructing Atlantic Intertropical Convergence Zone variability: Influence of the local cross-equatorial sea surface temperature gradient and remote forcing from the eastern equatorial Pacific. *Journal of Geophysical Research*, *107*(D1), ACL 3-1–ACL 3-19. https://doi.org/10.1029/2000JD000307

Climate Variability and Change Working Group (CVCWG). (2020a). CAM5 Prescribed SST AMIP Ensembles [Dataset]. *NCAR Climate Data Gateway*. Retrieved from https://www.cesm.ucar.edu/working-groups/climate/simulations/cam5-prescribed-sst

Climate Variability and Change Working Group (CVCWG). (2020b). CAM6 Prescribed SST AMIP Ensembles [Dataset]. *NCAR Climate Data Gateway*. Retrieved from https://www.cesm.ucar.edu/working-groups/climate/simulations/cam6-prescribed-sst

Dai, A. (2013). The influence of the inter-decadal Pacific oscillation on US precipitation during 1923–2010. *Climate Dynamics*, *41*(3–4), 633–646. https://doi.org/10.1007/s00382-012-1446-5

Dai, A., & Wigley, T. M. L. (2000). Global patterns of ENSO-induced precipitation. *Geophysical Research Letters*, *27*(9), 1283–1286. https://doi.org/10.1029/1999GL011140

Danabasoglu, G., Lamarque, J.-F., Bacmeister, J., Bailey, D. A., DuVivier, A. K., Edwards, J., et al. (2020). The Community Earth System Model Version 2 (CESM2). *Journal of Advances in Modeling Earth Systems*, *12*(2), e2019MS001916. https://doi.org/10.1029/2019MS001916

Dong, B., & Dai, A. (2015). The influence of the Interdecadal Pacific Oscillation on temperature and precipitation over the globe. *Climate Dynamics*, *45*(9–10), 2667–2681. https://doi.org/10.1007/s00382-015-2500-x

Dong, B., Dai, A., Vuille, M., & Elison Timm, O. (2018). Asymmetric modulation of ENSO teleconnections by the interdecadal Pacific oscillation. *Journal of Climate*, *31*(18), 7337–7361. https://doi.org/10.1175/JCLI-D-17-0663.1

Efron, B. (1979). Bootstrap methods: Another look at the jackknife. *The Annals of Statistics*, *7*(1), 1–26. https://doi.org/10.1214/aos/1176344552

Enfield, D. B., Mestas-Nuñez, A. M., & Trimble, P. J. (2001). The Atlantic Multidecadal Oscillation and its relation to rainfall and river flows in the continental U.S. *Geophysical Research Letters*, *28*(10), 2077–2080. https://doi.org/10.1029/2000GL012745

Espinoza, J. C., Segura, H., Ronchail, J., Drapeau, G., & Gutierrez-Cori, O. (2016). Evolution of wet-day and dry-day frequency in the western Amazon basin: Relationship with atmospheric circulation and impacts on vegetation. *Water Resources Research*, *52*(11), 8546–8560. https://doi.org/10.1002/2016WR019305

Flantua, S. G. A., Hooghiemstra, H., Vuille, M., Behling, H., Carson, J. F., Gosling, W. D., et al. (2016). Climate variability and human impact in South America during the last 2000 years: Synthesis and perspectives from pollen records. *Climate of the Past*, *12*(2), 483–523. https://doi.org/10.5194/cp-12-483-2016

Folland, C. K., Parker, D. E., & Kates, F. E. (1984). Worldwide marine temperature fluctuations 1856–1981. *Nature*, *310*(5979), 670–673. https://doi.org/10.1038/310670a0

Garreaud, R. D., Vuille, M., Compagnucci, R., & Marengo, J. (2009). Present-day South American climate. *Palaeogeography, Palaeoclimatology, Palaeoecology*, *281*(3–4), 180–195. https://doi.org/10.1016/j.palaeo.2007.10.032

GISTEMP Team. (2024). GISS Surface Temperature Analysis (GISTEMP), version 4 [Dataset]. *NASA Goddard Institute for Space Studies*. Retrieved from https://data.giss.nasa.gov/gistemp/

Grimm, A. M. (2003). The El Niño impact on the summer monsoon in Brazil: Regional processes versus remote influences. *Journal of Climate*, *16*(2), 263–280. https://doi.org/10.1175/1520-0442(2003)016<0263:TENIOT>2.0.CO;2

Grimm, A. M. (2011). Interannual climate variability in South America: Impacts on seasonal precipitation, extreme events, and possible effects of climate change. *Stochastic Environmental Research and Risk Assessment*, *25*(4), 537–554. https://doi.org/10.1007/s00477-010-0420-1

Grimm, A. M., Laureanti, N. C., Rodakoviski, R. B., & Gama, C. B. (2016). Interdecadal variability and extreme precipitation events in South America during the monsoon season. *Climate Research*, *68*(2–3), 277–294. https://doi.org/10.3354/cr01375

Grimm, A. M., Pal, J. S., & Giorgi, F. (2007). Connection between spring conditions and peak summer monsoon rainfall in South America: Role of soil moisture, surface temperature, and topography in eastern Brazil. *Journal of Climate*, *20*(24), 5929–5945. https://doi.org/10.1175/2007JCLI1684.1

Grimm, A. M., & Saboia, J. P. J. (2015). Interdecadal variability of the South American precipitation in the monsoon season. *Journal of Climate*, *28*(2), 755–775. https://doi.org/10.1175/JCLI-D-14-00046.1

Grimm, A. M., & Silva Dias, P. L. (1995). Analysis of tropical–extratropical interactions with influence functions of a barotropic model. *Journal of the Atmospheric Sciences*, *52*(20), 3538–3555. https://doi.org/10.1175/1520-0469(1995)052<3538:AOTIWI>2.0.CO;2

Harris, I., Osborn, T. J., Jones, P., & Lister, D. (2020). Version 4 of the CRU TS monthly high-resolution gridded multivariate climate dataset. *Scientific Data*, *7*, 109. https://doi.org/10.1038/s41597-020-0453-3

Hastenrath, S., & Heller, L. (1977). Dynamics of climatic hazards in northeast Brazil. *Quarterly Journal of the Royal Meteorological Society*, *103*(435), 77–92. https://doi.org/10.1002/qj.49710343505

He, C., Clement, A. C., Kramer, S. M., Cane, M. A., Klavans, J. M., Fenske, T. M., & Murphy, L. N. (2023). Tropical Atlantic multidecadal variability is dominated by external forcing. *Nature*, *622*(7983), 521–527. https://doi.org/10.1038/s41586-023-06489-4

He, Z., Dai, A., & Vuille, M. (2021). The joint impacts of Atlantic and Pacific multidecadal variability on South American precipitation and temperature. *Journal of Climate*, *34*(19), 7959–7981. https://doi.org/10.1175/JCLI-D-21-0081.1

Henley, B. J., Gergis, J., Karoly, D. J., Power, S., Kennedy, J., & Folland, C. K. (2015). A tripole index for the Interdecadal Pacific Oscillation. *Climate Dynamics*, *45*(11–12), 3077–3090. https://doi.org/10.1007/s00382-015-2525-1

Hersbach, H., Bell, B., Berrisford, P., Biavati, G., Horányi, A., Muñoz Sabater, J., et al. (2023a). ERA5 monthly averaged data on pressure levels from 1940 to present [Dataset]. *Copernicus Climate Change Service (C3S) Climate Data Store (CDS)*. https://doi.org/10.24381/cds.6860a573

Hersbach, H., Bell, B., Berrisford, P., Biavati, G., Horányi, A., Muñoz Sabater, J., et al. (2023b). ERA5 monthly averaged data on single levels from 1940 to present [Dataset]. *Copernicus Climate Change Service (C3S) Climate Data Store (CDS)*. https://doi.org/10.24381/cds.f17050d7

Horel, J. D., & Wallace, J. M. (1981). Planetary-scale atmospheric phenomena associated with the Southern Oscillation. *Monthly Weather Review*, *109*(4), 813–829. https://doi.org/10.1175/1520-0493(1981)109<0813:PSAPAW>2.0.CO;2

Hua, W., Dai, A., Zhou, L., Qin, M., & Chen, H. (2019). An externally forced decadal rainfall seesaw pattern over the Sahel and southeast Amazon. *Geophysical Research Letters*, *46*(2), 923–932. https://doi.org/10.1029/2018GL081406

Huang, B., Banzon, V. F., Freeman, E., Lawrimore, J., Liu, W., Peterson, T. C., et al. (2015). Extended Reconstructed Sea Surface Temperature (ERSST), version 4 [Dataset]. *NOAA National Centers for Environmental Information*. https://doi.org/10.7289/V5KD1VVF

Huang, B., Thorne, P. W., Banzon, V. F., Boyer, T., Chepurin, G., Lawrimore, J. H., et al. (2017). NOAA Extended Reconstructed Sea Surface Temperature (ERSST), version 5 [Dataset]. *NOAA National Centers for Environmental Information*. https://doi.org/10.7289/V5T72FNM

Jiménez-Muñoz, J. C., Mattar, C., Barichivich, J., Santamaría-Artigas, A., Takahashi, K., Malhi, Y., et al. (2016). Record-breaking warming and extreme drought in the Amazon rainforest during the course of El Niño 2015–2016. *Scientific Reports*, *6*, 33130. https://doi.org/10.1038/srep33130

Johnson, Z. F., Chikamoto, Y., Wang, S.-Y. S., McPhaden, M. J., & Mochizuki, T. (2020). Pacific decadal oscillation remotely forced by the equatorial Pacific and the Atlantic Oceans. *Climate Dynamics*, *55*(3–4), 789–811. https://doi.org/10.1007/s00382-020-05295-2

Karoly, D. J. (1989). Southern Hemisphere circulation features associated with El Niño-Southern Oscillation events. *Journal of Climate*, *2*(11), 1239–1252. https://doi.org/10.1175/1520-0442(1989)002<1239:SHCFAW>2.0.CO;2

Kayano, M. T., Cerón, W. L., Andreoli, R. V., Souza, R. A. F., Avila-Diaz, A., Zuluaga, C. F., & Carvalho, L. M. V. (2022). Does the El Niño-Southern Oscillation affect the combined impact of the Atlantic Multidecadal Oscillation and Pacific Decadal Oscillation on the precipitation and surface air temperature variability over South America? *Atmosphere*, *13*(2), 231. https://doi.org/10.3390/atmos13020231

Knight, J. R., Folland, C. K., & Scaife, A. A. (2006). Climate impacts of the Atlantic Multidecadal Oscillation. *Geophysical Research Letters*, *33*(17), L17706. https://doi.org/10.1029/2006GL026242

Lenssen, N. J. L., Schmidt, G. A., Hansen, J. E., Menne, M. J., Persin, A., Ruedy, R., & Zyss, D. (2019). Improvements in the GISTEMP uncertainty model. *Journal of Geophysical Research: Atmospheres*, *124*(12), 6307–6326. https://doi.org/10.1029/2018JD029522

Lewis, S. L., Brando, P. M., Phillips, O. L., van der Heijden, G. M. F., & Nepstad, D. (2011). The 2010 Amazon drought. *Science*, *331*(6017), 554. https://doi.org/10.1126/science.1200807

Liu, Z. (2012). Dynamics of interdecadal climate variability: A historical perspective. *Journal of Climate*, *25*(6), 1963–1995. https://doi.org/10.1175/2011JCLI3980.1

Maksic, J., Shimizu, M. H., Kayano, M. T., Chiessi, C. M., Prange, M., & Sampaio, G. (2022). Influence of the Atlantic Multidecadal Oscillation on South American atmosphere dynamics and precipitation. *Atmosphere*, *13*(11), 1778. https://doi.org/10.3390/atmos13111778

Malhi, Y., Roberts, J. T., Betts, R. A., Killeen, T. J., Li, W., & Nobre, C. A. (2008). Climate change, deforestation, and the fate of the Amazon. *Science*, *319*(5860), 169–172. https://doi.org/10.1126/science.1146961

Marengo, J. A., Nobre, C. A., Tomasella, J., Oyama, M. D., de Oliveira, G. S., de Oliveira, R., et al. (2008). The drought of Amazonia in 2005. *Journal of Climate*, *21*(3), 495–516. https://doi.org/10.1175/2007JCLI1600.1

Marengo, J. A., Tomasella, J., Alves, L. M., Soares, W. R., & Rodriguez, D. A. (2011). The drought of 2010 in the context of historical droughts in the Amazon region. *Geophysical Research Letters*, *38*(12), L12703. https://doi.org/10.1029/2011GL047436

Meehl, G. A., Hu, A., Castruccio, F., England, M. H., Bates, S. C., Danabasoglu, G., et al. (2021). Atlantic and Pacific tropics connected by mutually interactive decadal-timescale processes. *Nature Geoscience*, *14*(1), 36–42. https://doi.org/10.1038/s41561-020-00669-x

Meehl, G. A., Shields, C., Arblaster, J. M., Annamalai, H., & Neale, R. (2020). Intraseasonal, seasonal, and interannual characteristics of regional monsoon simulations in CESM2. *Journal of Advances in Modeling Earth Systems*, *12*(6), e2019MS001962. https://doi.org/10.1029/2019ms001962

Mo, K. C., & Paegle, J. N. (2001). The Pacific–South American modes and their downstream effects. *International Journal of Climatology*, *21*(10), 1211–1229. https://doi.org/10.1002/joc.685

Moss, R. H., Edmonds, J. A., Hibbard, K. A., Manning, M. R., Rose, S. K., van Vuuren, D. P., et al. (2010). The next generation of scenarios for climate change research and assessment. *Nature*, *463*(7282), 747–756. https://doi.org/10.1038/nature08823

Neale, R. B., Gettelman, A., Park, S., Chen, C.-C., Lauritzen, P. H., Williamson, D. L., et al. (2012). *Description of the NCAR Community Atmosphere Model (CAM 5.0) (NCAR Technical Notes NCAR/TN-486+STR)*. National Center of Atmospheric Research. https://doi.org/10.5065/wgtk-4g06

Nobre, P., & Shukla, J. (1996). Variations of sea surface temperature, wind stress, and rainfall over the tropical Atlantic and South America. *Journal of Climate*, *9*(10), 2464–2479. https://doi.org/10.1175/1520-0442(1996)009%3C2464:VOSSTW%3E2.0.CO;2

O'Neill, B. C., Kriegler, E., Ebi, K. L., Kemp-Benedict, E., Riahi, K., Rothman, D. S., et al. (2017). The roads ahead: Narratives for shared socioeconomic pathways describing world futures in the 21st century. *Global Environmental Change*, *42*, 169–180. https://doi.org/10.1016/j.gloenvcha.2015.01.004

O'Neill, B. C., Kriegler, E., Riahi, K., Ebi, K. L., Hallegatte, S., Carter, T. R., et al. (2014). A new scenario framework for climate change research: The concept of shared socioeconomic pathways. *Climatic Change*, *122*(3), 387–400. https://doi.org/10.1007/s10584-013-0905-2

Power, S., Casey, T., Folland, C., Colman, A., & Mehta, V. (1999). Inter-decadal modulation of the impact of ENSO on Australia. *Climate Dynamics*, *15*(5), 319–324. https://doi.org/10.1007/s003820050284

Qin, M., Dai, A., & Hua, W. (2020). Quantifying contributions of internal variability and external forcing to Atlantic multidecadal variability since 1870. *Geophysical Research Letters*, *47*(22), e2020GL089504. https://doi.org/10.1029/2020GL089504

Rayner, N. A., Parker, D. E., Horton, E. B., Folland, C. K., Alexander, L. V., Rowell, D. P., et al. (2003). Global analyses of sea surface temperature, sea ice, and night marine air temperature since the late nineteenth century. *Journal of Geophysical Research*, *108*(D14), 4407. https://doi.org/10.1029/2002JD002670

Ruprich-Robert, Y., Moreno-Chamarro, E., Levine, X., Bellucci, A., Cassou, C., Castruccio, F., et al. (2021). Impacts of Atlantic multidecadal variability on the tropical Pacific: A multi-model study. *Npj Climate and Atmospheric Science*, *4*, 33. https://doi.org/10.1038/s41612-021-00188-5

Ruprich-Robert, Y., Msadek, R., Castruccio, F., Yeager, S., Delworth, T., & Danabasoglu, G. (2017). Assessing the climate impacts of the observed Atlantic multidecadal variability using the GFDL CM2.1 and NCAR CESM1 global coupled models. *Journal of Climate*, *30*(8), 2785–2810. https://doi.org/10.1175/JCLI-D-16-0127.1

Salazar, A., Baldi, G., Hirota, M., Syktus, J., & McAlpine, C. (2015). Land use and land cover change impacts on the regional climate of non-Amazonian South America: A review. *Global and Planetary Change*, *128*, 103–119. https://doi.org/10.1016/j.gloplacha.2015.02.009

Sasaki, W., Doi, T., Richards, K. J., & Masumoto, Y. (2015). The influence of ENSO on the equatorial Atlantic precipitation through the Walker circulation in a CGCM. *Climate Dynamics*, *44*(1–2), 191–202. https://doi.org/10.1007/s00382-014-2133-5

Schlesinger, M. E., & Ramankutty, N. (1994). An oscillation in the global climate system of period 65–70 years. *Nature*, *367*(6465), 723–726. https://doi.org/10.1038/367723a0

Schneider, U., Hänsel, S., Finger, P., Rustemeier, E., & Ziese, M. (2022). GPCC Full Data Monthly Product version 2022 at 0.5°: Monthly land-surface precipitation from rain-gauges built on GTS-based and historical data [Dataset]. *Global Precipitation Climatology Centre*. https://doi.org/10.5676/DWD_GPCC/FD_M_V2022_050

Slivinski, L. C., Compo, G. P., Whitaker, J. S., Sardeshmukh, P. D., Giese, B. S., McColl, C., et al. (2019). Towards a more reliable historical reanalysis: Improvements for version 3 of the Twentieth Century Reanalysis system. *Quarterly Journal of the Royal Meteorological Society*, *145*(724), 2876–2908. https://doi.org/10.1002/qj.3598

Sutton, R. T., McCarthy, G. D., Robson, J., Sinha, B., Archibald, A. T., & Gray, L. J. (2018). Atlantic multidecadal variability and the U.K. ACSIS program. *Bulletin of the American Meteorological Society*, *99*(2), 415–425. https://doi.org/10.1175/BAMS-D-16-0266.1

Tedeschi, R. G., Grimm, A. M., & Cavalcanti, I. F. A. (2015). Influence of Central and East ENSO on extreme events of precipitation in South America during austral spring and summer. *International Journal of Climatology*, *35*(8), 2045–2064. https://doi.org/10.1002/joc.4106

Trenberth, K. E., & Shea, D. J. (2005). Relationships between precipitation and surface temperature. *Geophysical Research Letters*, *32*(14), L14703. https://doi.org/10.1029/2005GL022760

Trenberth, K. E., & Shea, D. J. (2006). Atlantic hurricanes and natural variability in 2005. *Geophysical Research Letters*, *33*(12), L12704. https://doi.org/10.1029/2006GL026894

Tropical Rainfall Measuring Mission (TRMM). (2011). TRMM (TMPA/3B43) Rainfall Estimate L3 1 month 0.25 degree x 0.25 degree V7 [Dataset]. *Goddard Earth Sciences Data and Information Services Center (GES DISC)*. https://doi.org/10.5067/TRMM/TMPA/MONTH/7

Villamayor, J., Ambrizzi, T., & Mohino, E. (2018). Influence of decadal sea surface temperature variability on northern Brazil rainfall in CMIP5 simulations. *Climate Dynamics*, *51*(1–2), 563–579. https://doi.org/10.1007/s00382-017-3941-1

Vuille, M., Franquist, E., Garreaud, R., Lavado Casimiro, W. S., & Cáceres, B. (2015). Impact of the global warming hiatus on Andean temperature. *Journal of Geophysical Research: Atmospheres*, *120*(9), 3745–3757. https://doi.org/10.1002/2015JD023126

Wallace, J. M., & Gutzler, D. S. (1981). Teleconnections in the geopotential height field during the Northern Hemisphere winter. *Monthly Weather Review*, *109*(4), 784–812. https://doi.org/10.1175/1520-0493(1981)109<0784:TITGHF>2.0.CO;2

Zeng, N., Yoon, J.-H., Marengo, J. A., Subramaniam, A., Nobre, C. A., Mariotti, A., & Neelin, J. D. (2008). Causes and impacts of the 2005 Amazon drought. *Environmental Research Letters*, *3*(1), 014002. https://doi.org/10.1088/1748-9326/3/1/014002

Zhang, R., & Delworth, T. L. (2007). Impact of the Atlantic Multidecadal Oscillation on North Pacific climate variability. *Geophysical Research Letters*, *34*(23), L23708. https://doi.org/10.1029/2007GL031601

Zhang, R., Sutton, R., Danabasoglu, G., Kwon, Y.-O., Marsh, R., Yeager, S. G., et al. (2019). A review of the role of the Atlantic Meridional Overturning Circulation in Atlantic Multidecadal Variability and associated climate impacts. *Reviews of Geophysics*, *57*(2), 316–375. https://doi.org/10.1029/2019RG000644

Zhang, Y., Wallace, J. M., & Battisti, D. S. (1997). ENSO-like interdecadal variability: 1900–93. *Journal of Climate*, *10*(5), 1004–1020. https://doi.org/10.1175/1520-0442(1997)010<1004:ELIV>2.0.CO;2

Zhou, J., & Lau, K.-M. (2001). Principal modes of interannual and decadal variability of summer rainfall over South America. *International Journal of Climatology*, *21*(13), 1623–1644. https://doi.org/10.1002/joc.700

Zomer, R. J., Xu, J., & Trabucco, A. (2022). Version 3 of the global aridity index and potential evapotranspiration database. *Scientific Data*, *9*, 409. https://doi.org/10.1038/s41597-022-01493-1

Zwiers, F. W. (1990). The effect of serial correlation on statistical inferences made with resampling procedures. *Journal of Climate*, *3*(12), 1452–1461. https://doi.org/10.1175/1520-0442(1990)003%3C1452:TEOSCO%3E2.0.CO;2